

MEASUREMENT AND SYNTHESIS OF THE TROMBONE, SFU

by

Frederick S. Scott

M.M., New York University, 2008

B.A., University of Nebraska (Lincoln), 2006

A THESIS SUBMITTED IN PARTIAL FULFILLMENT
OF THE REQUIREMENTS FOR THE DEGREE OF
MASTER OF SCIENCE
in the
School of Computing Science
Faculty of Applied Sciences

© Frederick S. Scott 2012
SIMON FRASER UNIVERSITY
Summer 2012

All rights reserved. However, in accordance with the Copyright Act of Canada, this work may be reproduced without authorization under the conditions for Fair Dealing. Therefore, limited reproduction of this work for the purposes of private study, research, criticism, review and news reporting is likely to be in accordance with the law, particularly if cited appropriately.

APPROVAL

Name: Frederick S. Scott
Degree: Master of Science
Title of thesis: Measurement and Synthesis of the Trombone, SFU

Examining Committee: Dr. Kay C. Wiese
Chair

Dr. Tamara Smyth, Assistant Professor, Computing
Science
Simon Fraser University
Senior Supervisor

Dr. Torsten Möller, Professor, Computing Science
Simon Fraser University
Supervisor

Dr. Mark Drew, Professor, Computing Science
Simon Fraser University
SFU Examiner

Date Approved: 21 August 2012

Partial Copyright Licence



The author, whose copyright is declared on the title page of this work, has granted to Simon Fraser University the right to lend this thesis, project or extended essay to users of the Simon Fraser University Library, and to make partial or single copies only for such users or in response to a request from the library of any other university, or other educational institution, on its own behalf or for one of its users.

The author has further granted permission to Simon Fraser University to keep or make a digital copy for use in its circulating collection (currently available to the public at the "Institutional Repository" link of the SFU Library website (www.lib.sfu.ca) at <http://summit.sfu.ca> and, without changing the content, to translate the thesis/project or extended essays, if technically possible, to any medium or format for the purpose of preservation of the digital work.

The author has further agreed that permission for multiple copying of this work for scholarly purposes may be granted by either the author or the Dean of Graduate Studies.

It is understood that copying or publication of this work for financial gain shall not be allowed without the author's written permission.

Permission for public performance, or limited permission for private scholarly use, of any multimedia materials forming part of this work, may have been granted by the author. This information may be found on the separately catalogued multimedia material and in the signed Partial Copyright Licence.

While licensing SFU to permit the above uses, the author retains copyright in the thesis, project or extended essays, including the right to change the work for subsequent purposes, including editing and publishing the work in whole or in part, and licensing other parties, as the author may desire.

The original Partial Copyright Licence attesting to these terms, and signed by this author, may be found in the original bound copy of this work, retained in the Simon Fraser University Archive.

Simon Fraser University Library
Burnaby, British Columbia, Canada

revised Fall 2011

Abstract

A physics-based model of the trombone is developed using filters derived both from theory and acoustical measurement. The measured filters are taken by extending a previously introduced measurement system, allowing for the isolation of the effects of the trombone bell, for which no known one dimensional traveling wave solution exists. The complete parametric model is coupled to a configurable generalized reed model and when properly set, the reed playability is strongly dependent on the bore and bell resonances. This synthesis is well suited for interactive, real time applications.

Contents

Approval	ii
Abstract	iii
Contents	iv
List of Tables	vi
List of Figures	vii
1 Introduction	1
1.1 Contributions and Motivation	1
1.2 Parametric Synthesis of Musical Instrument Sound	2
1.2.1 Signal-based Synthesis	2
1.2.2 Physics-based Synthesis	3
2 Trombone Instrument Model	7
2.1 Waveguide Model of an Acoustic Tube	7
2.2 Waveguide Model of a Trombone	9
2.3 Piecewise Approximation for Modeling the Bell	11
3 Measuring Trombone Waveguide Filter Elements	15
3.1 Linear Time Invariant Systems	15
3.2 Measuring LTI Systems	16
3.3 Measurement Setup	18
3.4 Measurement Data	19
3.5 Appending the Bell	24

3.6	Frequency Response of the Instrument Model	26
4	Coupling Lip and Instrument Models	31
4.1	The Lip Reed	31
4.2	Mouthpiece Formulation	39
5	Conclusion	44
5.1	Future Work	45
	Bibliography	47

List of Tables

2.1	Trombone tubular sections (numbers correspond to parts in Figures 2.4 and 2.4), including top (t.) and bottom (b.) inner and outer slides, retracted and extended (ext.)	10
2.2	Parameters for Bessel horn described by (2.4) that best fit the provided trombone bell.	13
4.1	Example valve parameters [15].	37
4.2	Mouthpiece parameter values [15].	39

List of Figures

2.1	The waveguide of an infinite lossless cylindrical tube.	8
2.2	Waveguide model of a trombone with commuted propagation loss filters $\lambda(z)$, bell flare reflection and transmission filters $R_B(z)$ and $T_B(z)$, respectively, and a reflection filter $R_M(z)$ at the (effectively) closed lip end. Pressure is input to system through $X(z)$ and two outputs are taken at $Y_M(z)$ and $Y_B(z)$, corresponding to the pressure inside of the tube's closed end and the pressure transmitted out of the open end, respectively [16].	9
2.3	Labeled exterior of the trombone with parts corresponding to Table 2.1. . . .	10
2.4	Labeled interior of the trombone with parts corresponding to Table 2.1. . . .	11
2.5	An illustration of a piecewise bell shape using conical or cylindrical sections. .	12
2.6	The profile of the bell shows a close fit to the equation for the Bessel horn, given in (2.4), using parameter from Table 2.2.	12
3.1	Photos of PVC pipe illustrating the locations of the speaker and microphone capsules. The interior microphone sits flush with the inner wall of the tube, seen in the image on the left. The speaker is placed on the same end as the interior microphone, seen in the middle image. The external microphone is placed 7 cm away from the open end of the tube, seen in the image on the right.	19
3.2	Closed Tube Arrivals.	20
3.3	Propagation Loss for Tube.	21
3.4	Open Tube, internal microphone arrivals..	22
3.5	Open Tube, external microphone arrivals.	22
3.6	Open End Reflection for Tube.	23
3.7	Open End Transmission for Tube.	24

3.8	The trombone bell appended to the measurement tube.	24
3.9	Tube with bell appended, internal microphone arrivals.	25
3.10	Tube with bell appended, external microphone arrivals.	26
3.11	Estimated and modeled bell reflection (top) and transmission (bottom) magnitudes.	27
3.12	Spectrum of the impulse responses of an ideal lossless closed cylindrical tube, the trombone model without a mouthpiece attached with a 39 Hz grid in black and a 60 Hz grid in red.	28
3.13	Spectrum of the impulse response of the trombone model without mouthpiece and the slide extended 50cm.	30
4.1	Configurations of Pressure Control Valve. 1. blown closed $(-, +)$, found in clarinets and saxophones. 2. longitudinally blown open $(+, -)$, found in trumpets and trombones. 3. transversely blown open $(+, +)$, found in the avian syrinx. [6].	32
4.2	Generalized Pressure Control Valve in the blown open configuration with a stop placed on the vertical axis at $\theta = 0$. Parameters λ_m and λ_b are lengths of the reed that are affected by the pressure from the mouth and bore, respectively. μ is the length of the valve that is affected by the volume flow. The forces on these surfaces change the angle of the valve opening, θ	33
4.3	Comparison of different ν values used in Equation 4.2.	34
4.4	Time domain plots of the volume flow, U ; reed displacement, θ ; internal bore pressure, y_0 ; and transmitted pressure, y_b . The outputs for the internal and transmitted pressure correspond to the waveguide model diagram in Figure 2.2.	36
4.5	Frequency domain plots of the volume flow, U ; reed displacement, θ ; internal bore pressure, y_0 ; and transmitted pressure, y_B . The outputs for the internal and transmitted pressure correspond to the waveguide model diagram in Figure 2.2.	38
4.6	Comparison between the frequency spectrum of the trombone instrument model without mouthpiece and the produced sound seen in Figures 4.4 and 4.5.	39

4.7	Illustration of a mouthpiece cross section, showing the cup shaped volume, V , attached to the conical choke, with length, l_c and an average radius, a_c . Values for these parameters can be found in Table 4.2.	40
4.8	The system diagram for the mouthpiece model. The cup volume is represented by the capacitor, and the attached narrow constriction is modeled as a series inertance L and dissipative element R [15].	40
4.9	Trombone model spectra with and without the mouthpiece.	42
4.10	Comparison between the frequency spectrum of the trombone instrument model with mouthpiece and a tone synthesized at 176 Hz.	43
5.1	Measurement appliance for the trombone inner slide with a microphone capsule flush with the cylinder wall and a backing plate for the mounting of a playback speaker.	46

Chapter 1

Introduction

1.1 Contributions and Motivation

This work contributes a physical synthesis model of the trombone, a virtual musical instrument emphasizing quality sound production and interactivity. It focuses on acoustic accuracy while remaining parametrically flexible by using a combination of elements that are modeled either based on known theory or, for elements not well described theoretically, from acoustical measurement. Though the trombone bore may be approximated with sufficient accuracy as a cylinder, an acoustic tube for which one-dimensional traveling waves are described theoretically, there is no known one dimensional traveling wave solution for the trombone bell. We extended an acoustical measurement technique to obtain the characteristic reflection and transmission filters of the trombone bell for use within a waveguide synthesis model. Previous efforts in brass instrument modeling, generally centered around the trumpet, have relied on either measured reflection functions of the entire instrument or have been purely theoretical approximations. Our hybrid method maintains the level of interaction desired in a virtual musical instrument, at the low computational cost of a waveguide model, while allowing acoustical accuracy from measured filter elements not expected to change during performance.

Physical modeling is used in this case because it is more informed by the acoustics governing the interaction between the instrument and the musician, unlike signal-based methods which model only the final produced sound. With this connection, the process of creating a physical model and configuring its parameters serves as a study of the instrument and how it is played. As a classically trained trombonist, this was what attracted me to

the research. Rather than creating a synthesizer with the goal of replacing musicians, it can serve as a tool to help trombonists further their understanding of the instrument and, with further work, be extended to augment the player's capabilities, for example, by using inverse modeling and parameter estimation to reconstruct the input to the instrument, which could then be used to drive a different virtual instrument.

1.2 Parametric Synthesis of Musical Instrument Sound

1.2.1 Signal-based Synthesis

Historically, several methods have been used to synthesize brass instrument tones. One of the most accurate methods, in terms of sound quality, is wavetable synthesis, where samples of the instrument being synthesized are recorded and then played back. Rather than attempting to prerecord the entire range of an instrument's expression, considering every variation and combination of pitch, loudness and tone quality, a limited number of samples are taken and then modified with various audio effects, such as pitch shifting, to cover the unsampled range. The problem is that with most instruments the spectrum is dynamic in ways not easily predicted or modeled with a basic mapping of input parameters. For example, changing the amplitude of a wavetable will alter the intensity but won't recreate the spectral differences that often occur when an instrument is played at different volumes. Problems such as this are often avoided by taking more samples but processing is still necessary to combine them into a continuum. Sampling can sound very lifelike but the illusion is broken if a lack of variety in the tone necessary for musical expression becomes apparent.

Sinusoidal modeling, also known as Fourier recombination, is a method whereby a signal is synthesized by summing sinusoids. This is possible considering Fourier's Theorem, which states that any bandlimited periodic signal can be reproduced as the sum of a finite number of sinusoids having varying amplitude, phase and frequency [12]. A target sound is analyzed with the Fourier transform to view its spectrum, from which the parameters for reconstruction can be gleaned. To view how the spectrum changes over time, a short-time Fourier transform, a sequence of Fourier transforms of a window sliding along the signal, is used. The challenge of sinusoidal modeling is finding a meaningful mapping between the observed temporal spectral evolution and the musical control parameters made available to the user. Though the method is more computationally expensive than wavetable synthesis,

it requires less storage as the analysis allows signals to be represented with considerably less data.

Another synthesis method is Frequency Modulation (FM), where the frequency of one or more carrier sinusoids is modified by one or more modulating sinusoids, creating side-band frequency components. This method was developed by John Chowning in the late 1960's and popularized with Yamaha's DX7 keyboard. By modifying the frequency and amplitude of the modulator and arranging the carriers and modulators in different network topologies, complex time-varying sounds can be produced at low computational cost. Developing proper configurations of oscillators and FM parameters is not so straight forward; however, several attempts with limited success have been made to automate the process of parameter estimation. The end result of FM synthesis, however, can be both convincing and computationally efficient. A sound created by frequency modulation using just two sinusoidal oscillators can create a very broad spectrum which would require several oscillators with sinusoidal modeling. Nevertheless, the issue of finding a mapping between user input (control parameters) and FM synthesis parameters recurs.

1.2.2 Physics-based Synthesis

In contrast to signal-based synthesis techniques which work by reproducing an observed signal regardless of the underlying governing physics, physical modeling produces sounds by simulating mechanical and acoustic wave propagation in an instrument being played. By simulating what is physically happening in the instrument many complex idiomatic behaviors emerge naturally, unlike in signal based methods where such behaviors must be explicitly modeled. For example the attack, or onset, of a tone, known to be perceptually significant for identifying particular instrument sounds, can create a widely varying spectrum before reaching the steady state. Though this would require a number of extra parameters and customization in a signal-based model, this behavior would naturally occur in a well formed physical model. Also rather than dealing with abstract, indirectly related synthesis parameters, the synthesis and control parameters correspond more directly, making them more intuitive to the user.

A common issue in musical instrument synthesis is the mapping of control parameters. An experienced player with a real instrument will have the ability to expressively control the spectrum produced by the instrument; when creating a model, or virtual instrument, the goal is not only to have it be able to recreate that wide variation in spectrum, but to

afford the user the ability to manipulate the model expressively, as with the real instrument. Though playability and control are not the focus of this work, mindfulness of these issues are necessary for further refinement of the model as a musical instrument.

Most commercial synthesizers are focused around the keyboard instrument paradigm of control: a discrete note on/off with set pitch and loudness. In contrast, with brass instruments the player controls the pitch, loudness, and spectral envelope continuously through the duration of a note. With physical models often the control parameters require little mapping to direct synthesis parameters but controlling them from a keyboard is problematic, especially for brass instrument models. Even with the added tools of pitch sliders, mod wheels and aftertouch control, a keyboard will either not be able to produce idiomatic gestures for brass instruments or use a mapping that will reproduce these gestures but limit the player's control.

One of the first physical models was of the human vocal tract, developed in 1961 by Kelly and Lochbaum working in the Bell Laboratories [13]. The model approximated the vocal tract shape with a piecewise connection of a number of small segments of various radii. The junctions between the segments model the change of acoustical impedance that occurs along a tube of varying cross section, which causes a reflection and transmission of the traveling wave. It's the arrangement of these reflections that create the formants, characteristic peaks in the magnitude spectrum, which allow a listener to distinguish one vowel sound from another even if spoken at the same pitch. This model served as a precursor to the waveguide model which was later used by Perry Cook for modeling the singing voice [13].

Another development was the Karplus-Strong plucked string in 1983, which used a feedback delay line initialized with noise to simulate the comb-filter-like nature of a plucked guitar string [8]. It produced a convincing sound, though only in a limited frequency range in the middle of the gamut, and its simplicity allowed it to be easily controlled. The model was extended by Smith and Jaffe [7] to be musically useful by adding a variety of filters to extend the usable range and help control the rate of decay and thus note durations.

These previous works lead to the formalization of the waveguide structure by Julius O. Smith [10] which served as the basis for many physical models to come. One of the significant brass waveguides was Cook's TBone, developed in 1991, which used a piecewise model for instrument coupled to a single moving mass to simulate the player's lips [3]. The model was extensively parametric, allowing for the instrument mouthpiece, bore and bell

to change size.

Rodet and Vergez introduced a trumpet model in 1996 that was similar to Cook's model in structure, but used a measured instrument reflection function [9]. Their reflection function originally consisted of a straight tube but was later expanded into a full measured impulse response of a trumpet. Normally the use of a whole instrument impulse response would limit the synthesis possibilities by locking the instrument into one state¹, but Rodet and Vergez identified a section between echos in their impulse response which could be lengthened or shortened, allowing them to change the instrument's effective length. This was simple, computationally efficient and served to change the pitch of the instrument model.

In physical modeling of brass instruments, Berners' 1999 PhD dissertation stands out [2]. It focuses on the theory behind modeling wave propagation in the parts of the instrument, particularly the exponential curve of the bell flare. The cylindrical and single conical sections, such as the trombone hand slide and tuning slide respectively, are relatively simple and thus, the majority of the work entails the modeling of the brass bell flare, specifically the Sturm-Liouville partial differential equations arising from the junctions of multiple conical sections.

Though there are many commercially available physical modeling synthesizers for other instruments, such as piano and strings, there is only a single prominent one for brass instruments, Arturia Brass [18]. This was developed in part with Institut de Recherche et Coordination Acoustique/Musique (IRCAM) researchers Vergez and Tisserand. Though the instrument model itself is described as being essentially the same one from Vergez's previous work with Rodet, its new contribution is with the parameters controlling the instrument. They were generated using simulated annealing optimization and then mapped for ease of use with standard midi control devices.

With the motivation to create a brass physical model discussed and their history explored, the rest of this work can delve into the creation of such a model. Chapter 2 will address one dimensional wave propagation in waveguide models, expanding into the physical models of acoustical tubes and culminating with the model of the trombone. Chapter 3 will examine linear time-invariant systems and impulse response theory to setting the groundwork to acoustically measure a tube and the trombone bell and derive filters for

¹The trumpet has 3 valves, creating the possibility of 8 different bore length, a manageable number of different impulse responses to record and then switch between. The trombone, on the other hand, has a moving slide, allowing for an infinite number of possible lengths.

them. Chapter 4 will complete the trombone model by attaching a mouthpiece which will be coupled to a model of the brass player's lip reed. The final chapter will summarize the results of the synthesis and conclude with the future extensions of this research.

Chapter 2

Trombone Instrument Model

2.1 Waveguide Model of an Acoustic Tube

The trombone consists primarily of a long cylindrical bore, of possible varying length, terminated by a bell, or a flared horn. The bore may be approximated as a pure cylindrical tube, a structure for which the acoustics are well described theoretically. To physically model the sound produced by the trombone, we model pressure waves traveling along the length of the bore. In open air these waves propagate in three dimensions, however, when confined to a cylindrical tube with a relatively small diameter in relation to the wavelength of musically useful frequencies, a model using one-dimensional wave propagation is sufficient to capture the behavior of the system.

In the one-dimensional model there are two pressure waves traveling in opposite directions along the bore, referred to in the literature and as the left, y_l , and right, y_r , traveling waves [13]. The actual physical pressure at any point along the bore can be viewed as the sum of these left and right traveling waves. This can be expressed mathematically using d'Alembert's solution to the one-dimensional wave equation [13]. The pressure y at time t and position x along the bore length is given by:

$$y(t, x) = y_r(t - x/c) + y_l(t + x/c), \quad (2.1)$$

where y_l and y_r are the left and right traveling waves respectively and, c is the speed of wave propagation.

Equation 2.1 is discretized by replacing the continuous time variable t with integer multiples of a sampling period T_s (the inverse of the sampling rate) and the continuous

spatial variable x with integer multiples of the spatial sampling interval X (the distance traveled during one time sample), yielding:

$$y(nT_s, mX) = y_r(nT_s - mX/c) + y_l(nT_s + mX/c), \quad (2.2)$$

where n and m are integers multiplying T_s and X , respectively.

Since the distance the wave propagates in one sample period is equal to the product of the wave speed and the sampling periods, i.e. $X = cT_s$, (2.2) can be reduced to:

$$\begin{aligned} y(nT_s, mX) &= y_r(nT_s - mX/c) + y_l(nT_s + mX/c), \\ &= y_r((n-m)T_s) + y_l((n+m)T_s), \end{aligned}$$

where the final equation is often given as

$$y(n) = y_r(n-m) + y_l(n+m), \quad (2.3)$$

with the T_s omitted, though implied. Equation (2.3) is a discrete-time representation of the wave equation that reduces to a function of one variable, rather than two, i.e. a function of time only rather than space and time, offering a computational savings that makes one-dimensional waveguide models very useful for real-time synthesis.

Equation 2.3 is the time-domain representation of a one-dimensional digital waveguide, a bi-directional delay line representing left and right traveling waves. In signal flow diagrams, as shown in Figure 2.1, this is often represented in the z domain, where z^{-M} represents a delay of M samples, the time required for the pressure wave to propagate along a given length and the maximum value of m from Equation (2.3)[10].

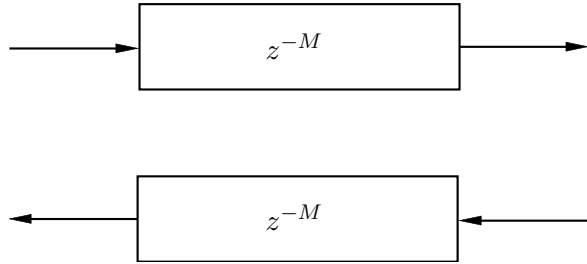


Figure 2.1: The waveguide of an infinite lossless cylindrical tube.

2.2 Waveguide Model of a Trombone

When modeling the trombone, the cylindrical tube simulating the bore can be given a finite length with boundary conditions at the mouthpiece/reed and bell and propagation losses due to viscous drag and thermal conduction that takes place in a thin layer along the bore walls [14]. Figure 2.2 shows such a model of a trombone bore that is predominantly closed by the lips on one end with reflection function R_M , and predominantly open on the other with the bell flare with reflection and transmission functions, R_B and T_B , respectively. These new elements are added to the waveguide segment from Figure 2.1 along with the wall/propagation losses, which, though distributed along the length of the bore, may be lumped into a single filter $\lambda(z)$ at the outputs of the delay lines [16]. The effects and formulation of these filters will be examined more closely in Chapter 3.

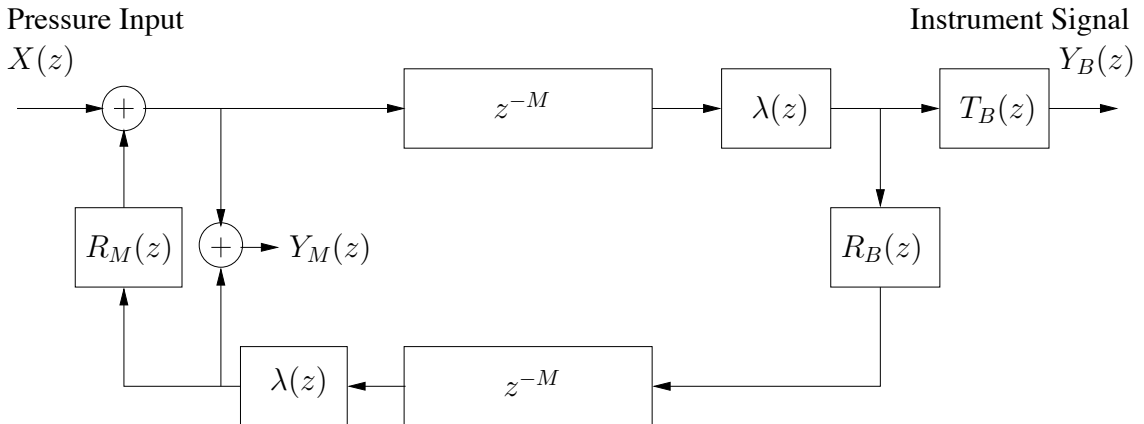


Figure 2.2: Waveguide model of a trombone with commuted propagation loss filters $\lambda(z)$, bell flare reflection and transmission filters $R_B(z)$ and $T_B(z)$, respectively, and a reflection filter $R_M(z)$ at the (effectively) closed lip end. Pressure is input to system through $X(z)$ and two outputs are taken at $Y_M(z)$ and $Y_B(z)$, corresponding to the pressure inside of the tube's closed end and the pressure transmitted out of the open end, respectively [16].

In reality, the trombone consists of a number of cylinders of varying radii as seen in Figures 2.3 and 2.4. It can be most accurately modeled as a series of waveguide sections joined with 2-port scattering junctions which account for the reflection and transmission that occurs when there is a change in the wave impedance, such as when a tube's cross-sectional area changes. Alternatively, the trombone's bore can be more simply modeled as a single cylinder with the effective length of the bore minus the bell (using values from Table

2.1 yields lengths of 209.1 cm with the hand slide fully retracted and 315.1 cm extended), using the model in Figure 2.2.

Part	Length (cm)	Radius (cm)
t. inner slide (1)	70.8	0.69
t. outer slide, ext. (2)	53	0.72
slide crook (3)	17.7	0.74
b. outer slide, ext. (4)	53	0.72
b. inner slide (5)	71.1	0.69
gooseneck (6)	24.1	0.71
tuning slide (7)	25.4	0.75,1.07
bell flare (8)	56.7	1,10.8

Table 2.1: Trombone tubular sections (numbers correspond to parts in Figures 2.4 and 2.4), including top (t.) and bottom (b.) inner and outer slides, retracted and extended (ext.).

For either model, the M value, for the z^{-M} delay line for each cylinder is selected by time required for the pressure wave to propagate along a given length. Though models using a piecewise bore and single cylinder were both implemented, there seemed to be no audible benefit to using multiple cylinders, and the latter offered more advantages in terms simplicity and usability.

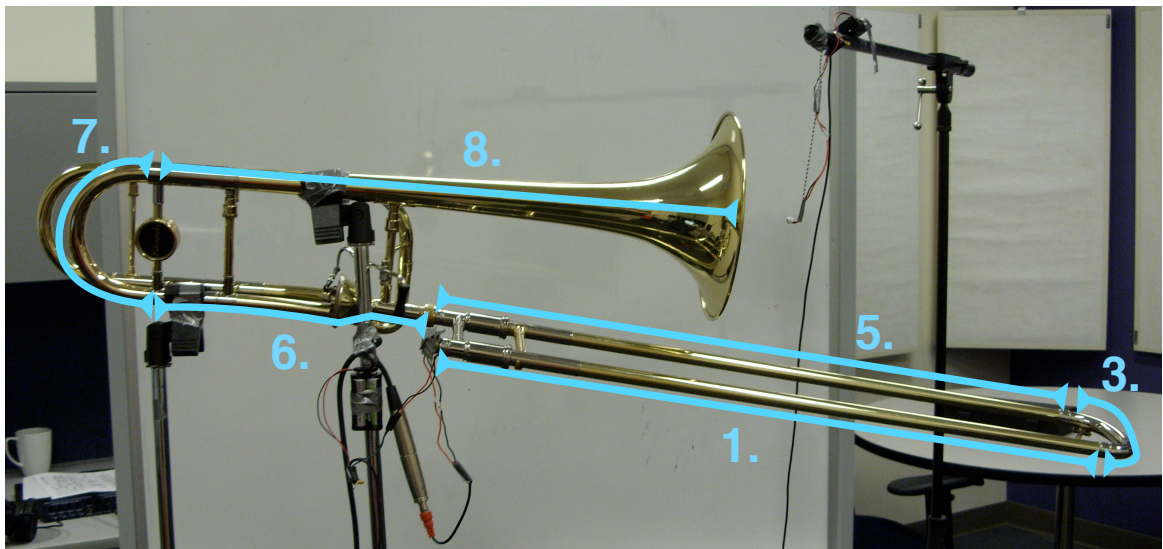


Figure 2.3: Labeled exterior of the trombone with parts corresponding to Table 2.1.

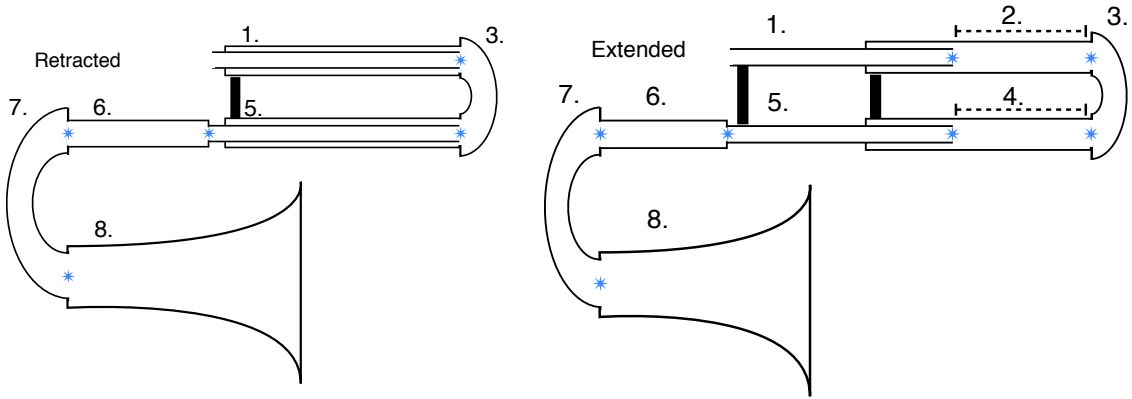


Figure 2.4: Labeled interior of the trombone with parts corresponding to Table 2.1.

2.3 Piecewise Approximation for Modeling the Bell

Though cones and cylinders may be accurately modeled using one-dimensional waveguides, the bell of the trombone, with its flared contour, has no known one dimensional traveling wave solution, due to its shape which causes continuous internal reflection and transmission as its cross-sectional area continuously changes. A number of one-dimensional approximations exist for the brass instrument bell flare but these will not capture the higher-order and evanescent modes inside of the bell [16].

A commonly used method is to approximate the bell with a piecewise connection of cylindrical and/or conical waveguide sections [2], as illustrated in Figure 2.5. A number of finite acoustic tubes are connected in series by scattering junctions, which model the reflection and transmission that occurs when a traveling wave encounters an impedance discontinuity that is created by the difference in cross-sectional area between adjacent tubes [13]. To best approximate the contour of the bell, the pure delay in each section is made as short as possible, only one sample in length.

The dimensions of each waveguide section are taken from the profile of the bell which is modeled by the Bessel horn,

$$a(x) = b(x + x_0)^{-\gamma}, \quad (2.4)$$

where x_0 is the position of the mouth of the horn, x is the distance from the horn mouth, and $a(x)$ is the radius over the length of the bell. The variables b and x_0 are chosen to give the correct radii at the small and large ends of the horn, while γ defines the rate of flare

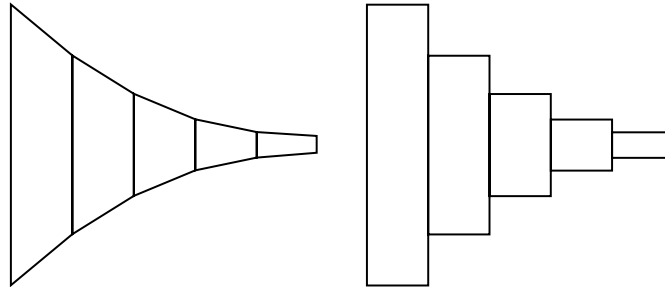


Figure 2.5: An illustration of a piecewise bell shape using conical or cylindrical sections.

[16]. Figure 2.6 shows a tight fit between the contours of the Bessel horn and the actual trombone bell profile using the parameters in Table 2.2.

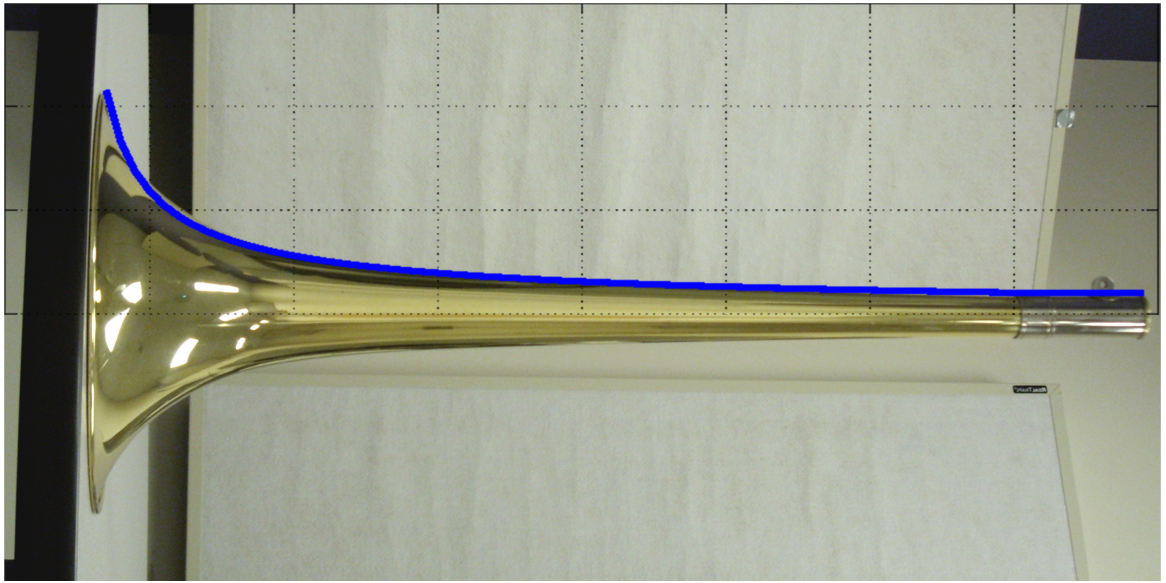


Figure 2.6: The profile of the bell shows a close fit to the equation for the Bessel horn, given in (2.4), using parameter from Table 2.2.

The piecewise bell model can be implemented in both time and frequency domains. In the latter, a matrix formulation allows for development of an expression describing the bell's reflection and transmission functions. The expression for the bell reflection function, R_B can be viewed as a transfer function, or the ratio of its output to its input, which is the

Quantity	Variable	Value
length of the bell (m)		.502
radius at bell mouth (m)		.108
radius at small end (m)		.01
bell flare constant	γ	.7
position of the bell mouth (m)	x_0	.0174
fitting parameter	b	0.0063

Table 2.2: Parameters for Bessel horn described by (2.4) that best fit the provided trombone bell.

ratio of the wave reflected by the bell p_1^- to the bell input wave p_1^+ , respectively, given by

$$\begin{aligned} R_B = \frac{p_1^-}{p_1^+} &= \lambda^2(\omega) \frac{p_N^+ \mathbf{P}_{2,1} + p_N^- \mathbf{P}_{2,2}}{p_N^+ \mathbf{P}_{1,1} + p_N^- \mathbf{P}_{1,2}}, \\ &= \lambda^2(\omega) \frac{\mathbf{P}_{2,1} + \mathbf{P}_{2,2} R_L(\omega)}{\mathbf{P}_{1,1} + \mathbf{P}_{1,2} R_L(\omega)}, \end{aligned} \quad (2.5)$$

where \mathbf{P} is a 4x4 matrix (for a 2-port scattering junction), the product of $N - 1$ scattering matrices, for N waveguide segments, where R_L is the cylindrical open-end reflection of the last segment [16].

Similarly, the bell transmission is given by the ratio of the wave radiated out the bell $p_N^+ T_L(\omega)$, where $T_L(\omega)$ is the cylindrical open-end transmission function, to the bell's input p_1^+ ,

$$T_B(\omega) = \frac{p_N^+ \lambda(\omega) T_L(\omega)}{p_1^+} = \frac{\lambda(\omega) T_L(\omega)}{\mathbf{P}_{1,1} + \mathbf{P}_{1,2} R_L(\omega)}. \quad (2.6)$$

Further details about the scattering matrix \mathbf{P} are beyond the scope of this work, but may be obtained in [16]. Expressions for calculating the cylindrical open-end reflection, R_L and transmission, T_L may be obtained in [14].

Though the piecewise model has the advantage of being parametric and thus changeable during performance of the virtual instrument, greater accuracy is expected through acoustic measurement. Theoretical filters are generally parametric, allowing them to adapt to changes in the instrument, i.e. if the trombone slide is extended a theoretical wall loss filter could be recalculated, compensating for the added length. Measured filters lack that flexibility but can provide greater accuracy, especially for the bell which is not expected

to change during performance. The next chapter, after providing groundwork in impulse response theory, details a method for measuring waveguide filter elements and compares these measurements to their theoretical counterparts.

Chapter 3

Measuring Trombone Waveguide Filter Elements

3.1 Linear Time Invariant Systems

Many acoustical systems can be approximated, with sufficient accuracy for sound synthesis, as being linear and time invariant (LTI). That is, if the effects of nonlinearities are deemed inaudible, they may be neglected for the sake of allowing the use of algorithms sufficiently efficient for interactive real-time parametric synthesis.

Given inputs $x(t)$ and $y(t)$, the system $\mathcal{L}_n(\omega)$ is linear if it satisfies distributive property, given by

$$\mathcal{L}_n(x(t) + y(t)) = \mathcal{L}_n(x(t)) + \mathcal{L}_n(y(t)). \quad (3.1)$$

That is, the same result is obtained when multiple signals are summed and input to the system as when signals are input separately and then summed at the output. To be linear, the system must also satisfy the commutative property,

$$X(z) \times \mathcal{L}_n(Y(z)) = \mathcal{L}_n(X(z)Y(z)), \quad (3.2)$$

which states that either may be multiplied to the input of the function or to the output of the function for the same result.

A system $\mathcal{L}_n(\omega)$ is time invariant if for input signal x ,

$$\mathcal{L}_n(x(n - N)) = \mathcal{L}_{n-N}(x(n)), \quad (3.3)$$

which says that no matter how far the input signal is shifted in time by N samples, the output will be the same, but just shifted in time [11].

The result of a system's linear time invariance is that it can only modify the amplitudes and phases of frequency components that are already present at its input; it cannot generate new frequency components.

If a system is both linear and time invariant it can be characterized in terms of an impulse response. That is, by exciting the system with an impulse and recording the response, we obtain all of the filter coefficients necessary to describe the system's frequency response.

In discrete time, an impulse is given by the Kronecker delta function,

$$\delta(n) = \begin{cases} 1, & n = 0 \\ 0, & n \neq 0, \end{cases} \quad (3.4)$$

where n are integer multiples of the sampling interval. The Kronecker delta contains all frequencies at equal amplitudes. This can be shown by taking its Discrete Fourier Transform (DFT),

$$\begin{aligned} X(\omega_k) &\triangleq \sum_{n=0}^{N-1} \delta(n) e^{-j(2\pi kn/N)} \\ &= \delta(0) e^{-j(2\pi k0/N)} \\ &= 1, \end{aligned} \quad (3.5)$$

regardless of the value of k .

Having an impulse at the input that contains equal energy for all frequencies in the bandwidth of interest ensures that the behavior of the LTI system is captured for that frequency range.

3.2 Measuring LTI Systems

When measuring impulse responses for LTI acoustic systems such as rooms it is common to approximate an impulse with a balloon pop or a starter gun. Though this can achieve good results, these methods are suited to measuring the response of large spaces but they

are impractical for some applications, such as measuring small tubes and instrument parts. The biggest problem is that, with such methods, the pulse created isn't reproducible, and thus it is difficult to obtain consistent results, meaning that though the impulse responses may be similar, they will not be exact with each measurement. For consistent impulse responses one must have a consistent impulse. To solve this problem, another method is to use a speaker to excite a system with a signal that is created and consistent.

Despite the ability to deliver a consistent signal, a speaker reproducing an impulse has a disadvantage of not being very loud due to the mechanical limitations of speaker technology. Driving a speaker with an impulse sufficiently loud to excite the system will likely distort the speaker and introduce artifacts in the impulse response. Having an impulse with sufficient amplitude to overcome the background noise in the system being measured is necessary for a measurement with an acceptable signal to noise ratio (SNR).

An alternative to driving the speaker with an impulse is to smear the impulse so that all frequencies are spread out over time. One of the most common methods for this is to use a sinusoid with a frequency that sweeps across the desired bandwidth [5]. The frequency is typically chosen to increase logarithmically over time to coincide with our perception of pitch. That is, though the range of human hearing is often cited as 20 Hz to 20,000 Hz we perceive the difference between 10,000 Hz to 20,000 Hz as having the same range of 100 Hz to 200 Hz. Given a listener's greater sensitivity to change in the lower frequencies, it is preferable to put equal amounts of energy for every doubling of frequency ¹ than to use a linear scale.

When the system under measurement is excited with a swept sine and the response that is recorded, post processing is needed to obtain the impulse response. To obtain an impulse, the frequency components of the sweep must be realigned as though they occurred at $t = 0$. Consider the transform of a swept sine $\sigma(\omega)$. If we divide $\sigma(\omega)$ by itself in the frequency domain,

$$\frac{\sigma(\omega)}{\sigma(\omega)} = 1 = DFT\{\delta(n)\}, \quad (3.6)$$

that is, we may take the inverse DFT to obtain $\delta(n)$. If $l(n)$ is response of an LTI system to a swept sine, to obtain the system's impulse response, $h(n)$, the swept sine is divided out in the frequency domain,

$$\frac{L(\omega)}{\sigma(\omega)} = H(\omega) = DFT\{h(n)\}. \quad (3.7)$$

¹In musical terms, this would be an octave.

This division in the frequency domain is called deconvolution.

If this deconvolution is done in the standard linear method, rather than circularly, it has the added benefit of removing any harmonic distortion being introduced by the speaker. As suggested by its name, harmonic distortion is a noise that is related to integer multiples of the fundamental of the original signal. In the case of a speaker being overdriven while playing a sinusoid at 100 Hz, there could be extraneous frequency components heard at 200 Hz, 300 Hz, 400 Hz and ascending upwards. This noise is correlated with the excitation signal and thus cannot be reduced by averaging multiple recordings, as is done to reduce uncorrelated background noise. Using circular deconvolution, these nonlinear responses will be perfectly aligned with the linear response. With linear deconvolution, however, the nonlinear responses for each harmonic are shifted in time before the linear response where they can be easily removed [5].

3.3 Measurement Setup

The trombone will be modeled with a waveguide similar to Figure 2.2 but we must first find filters for the bell reflection and transmission by measuring the impulse response of a trombone bell. Unfortunately this is not as simple as attaching a speaker to the bell and recording. It is important to remember that an impulse response contains the effects of every element in the signal chain, e.g. the speaker and microphone's individual frequency responses. We must be able to remove the unwanted parts of the system, such as the speaker response, to isolate the filters we need. This can be done by viewing the system being measured as a waveguide and analyzing the left and right traveling waves propagating through it. If the propagation delay of the tube is longer than the response length of the filters in the waveguide, the individual echos could be easily separable and analyzed.

To have a system with propagation delay that is relatively long compared to the length of filters involved, a 2 meter PVC cylinder was used as the basis for the measurement system. From recording its impulse responses, the filters simulating the tube's wall losses $\lambda(\omega)$ and open end reflection $R_L(\omega)$ can be estimated. Comparing these estimated filters to their well known theoretical counterparts could serve to validate the measurement technique, thus allowing new unknown filters to be estimated. At the end of the tube, on one side, there is a hole drilled in the wall that allows for a small microphone capsule, model JL-061C, to be placed flush with both the interior wall of cylinder and also the end of the tube lengthwise,

as seen in Figure 3.1. A small speaker, CUI Inc. CMS020KLX, fits flush on this end of the tube. On the other end another microphone capsule, model JL-061C, is suspended 7 cm from the open end, centered in the cylinder's cross sectional area. Two impulse responses are recorded: O from the microphone co-located with the speaker and O_E from the open end microphone. The open end is then terminated with a piece of plastic, providing near perfect reflection and response C is recorded from the co-located microphone.

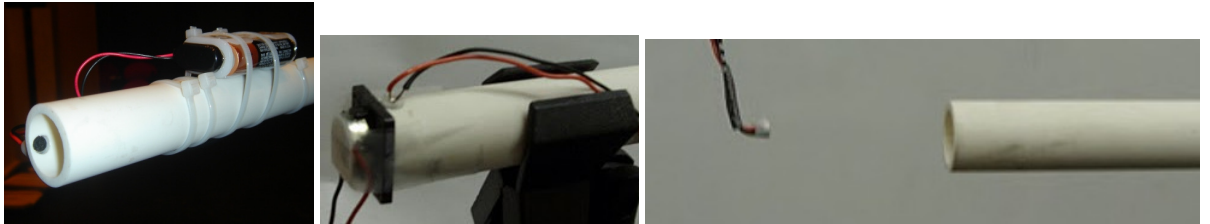


Figure 3.1: Photos of PVC pipe illustrating the locations of the speaker and microphone capsules. The interior microphone sits flush with the inner wall of the tube, seen in the image on the left. The speaker is placed on the same end as the interior microphone, seen in the middle image. The external microphone is placed 7 cm away from the open end of the tube, seen in the image on the right.

3.4 Measurement Data

It is important to remember that the impulse response captures the effects of everything present in the recording signal chain. The recorded impulse response contains the effects of the speaker and microphones involved if left untouched. This can be eliminated with inverse filtering. Because of the speaker and microphone positions used in this setup, the sound from the speaker arrives immediately to the microphone with minimal interference giving us the unadulterated response of the speaker and microphone combination. Once isolated this can be inverse filtered from the recorded response, leaving the response of just the tube itself. This new response can be used for synthesis but it is rigid and inflexible. It would be much more useful and enlightening if the individual effects of the different elements of the tube could be discerned [14].

Examining the tubes response in Figures 3.2 and 3.4, multiple distinct individual arrivals can be seen. These are evenly spaced at distances corresponding the time sound takes to travel to one end of the tube and back. Given the small radius of the tube it is known that musically useful frequencies propagate in one dimension inside the tube. Considering the

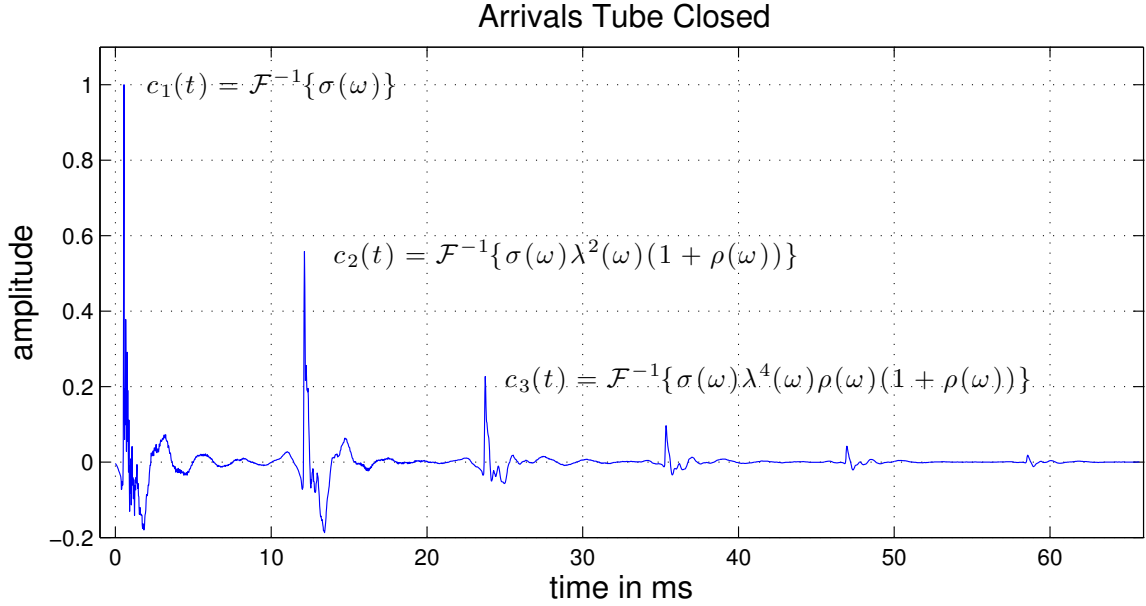


Figure 3.2: Closed Tube Arrivals.

one dimensional propagation, the pressure at any point inside of the tube can be viewed as the sum of the two waves, one traveling away from the speaker end, $+$, and one coming towards it, $-$.

Looking at the closed tube response in Figure 3.2, three things affect the wave propagation: the reflection off of the closed end, assumed to be 1; the reflection off of the speaker, $\rho(\omega)$; and thermoviscous wall losses related to the distance traveled, $\lambda(\omega)$. The closed end was made to be as near to perfectly reflective as possible. With this in mind the 2nd arrival at the speaker is the sum of the $+$ and $-$ waves:

$$C_2^- = \sigma(\omega)\lambda^2(\omega), \quad (3.8)$$

$$C_2^+ = \sigma(\omega)\lambda^2(\omega)\rho(\omega), \quad (3.9)$$

$$C_2 = C_2^+ + C_2^- = \sigma(\omega)\lambda^2(\omega)(1 + \rho(\omega)). \quad (3.10)$$

The Speaker Output $\sigma(\omega)$ has already been isolated in the 1st arrival but to isolate the Speaker Reflection $\rho(\omega)$ and the Wall Losses $\lambda(\omega)$ we must look at the third reflection, C3.

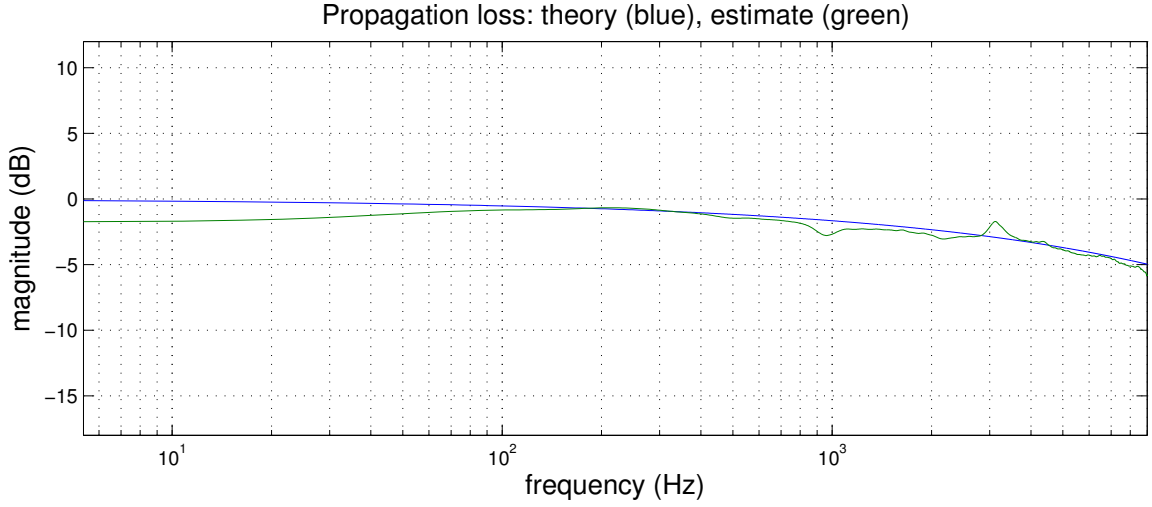


Figure 3.3: Propagation Loss for Tube.

This can be seen as related to C2 but with an additional roundtrip of wall losses and an additional time through the speaker reflection:

$$C_3 = \sigma(\omega)\lambda^4(\omega)\rho(\omega)(1 + \rho(\omega)). \quad (3.11)$$

Through algebraic manipulation of a temporary variable, $\zeta(\omega)$, can be created from ratios of the reflections:

$$\zeta(\omega) = \frac{C_1 C_3}{(C_2)^2} = \frac{\rho(\omega)}{1 + \rho(\omega)}, \quad (3.12)$$

From here the speaker reflection can be estimated:

$$\hat{\rho}(\omega) = \frac{\zeta(\omega)}{1 - \zeta(\omega)}, \quad (3.13)$$

With that the round trip wall losses can be discerned from a combination of the 2nd and 3rd arrivals:

$$\hat{\lambda}^2(\omega) = \frac{C_3}{\hat{\rho}(\omega)C_2}. \quad (3.14)$$

With the open end tube there is an additional filter to isolate, R_L , the reflection from the open end of the line, but because all of the other filters remain the same, it is easy to isolate this out as a ratio of the two arrivals:

$$\hat{R}_L(\omega) = \frac{O_2}{C_2} = \frac{\sigma(\omega)\lambda^2(\omega)R_L(\omega)(1 + \rho(\omega))}{\sigma(\omega)\lambda^2(\omega)(1 + \rho(\omega))}. \quad (3.15)$$

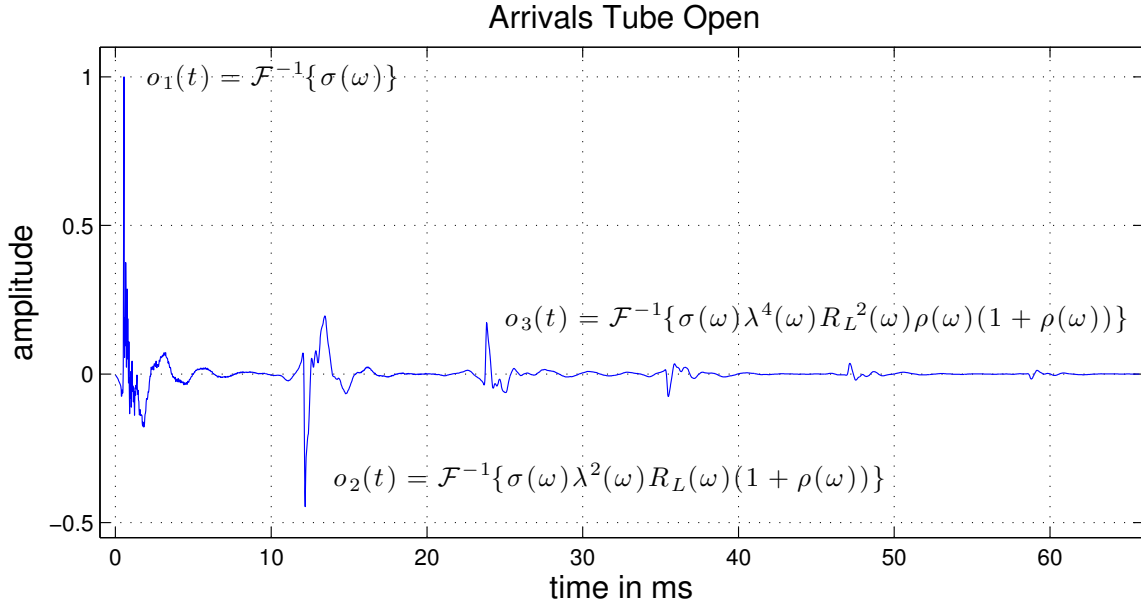


Figure 3.4: Open Tube, internal microphone arrivals..

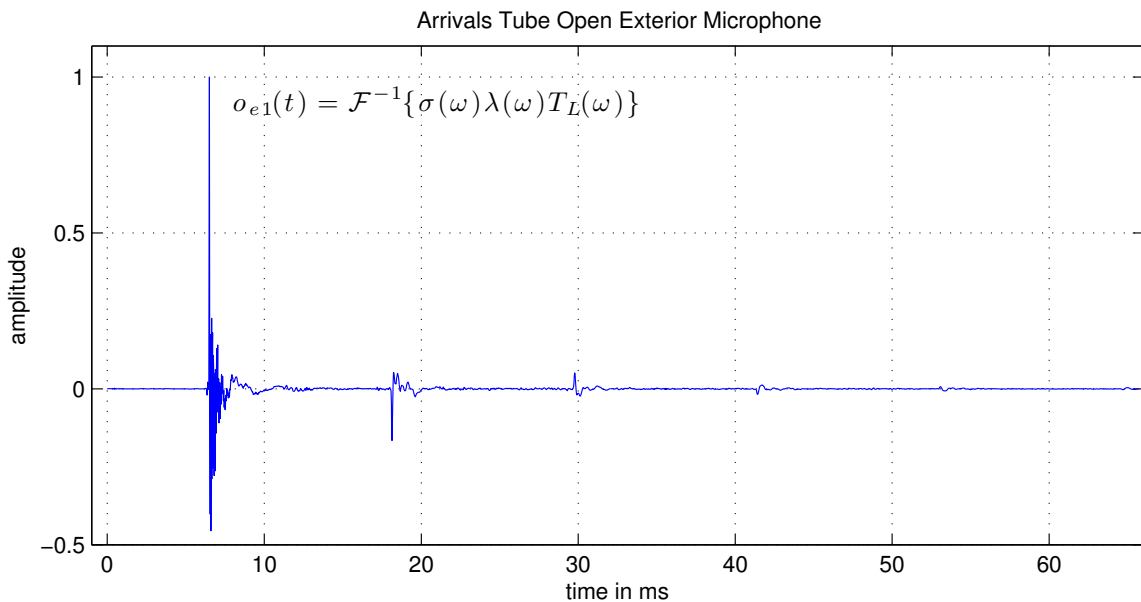


Figure 3.5: Open Tube, external microphone arrivals.

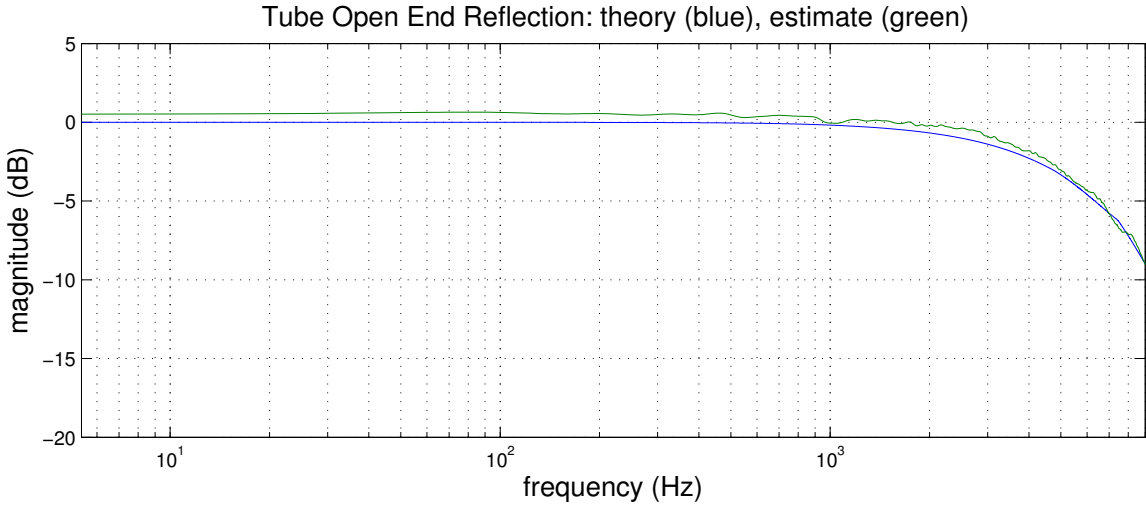


Figure 3.6: Open End Reflection for Tube.

Using the recordings taken from the microphone placed outside of the open end of the tube, the transmission filter can also be estimated. The 1st arrival at the external microphone can be viewed as:

$$O_{E1}(\omega) = \sigma(\omega)\lambda(\omega)T_L(\omega) \quad (3.16)$$

So to obtain the T_L :

$$T_L(\omega) = \frac{O_{E1}(\omega)}{\sigma(\omega)\lambda(\omega)} \quad (3.17)$$

The estimated filters for the tube's propagation losses are within a few decibels of the theoretical loss filters through the 100 Hz to 10,000 Hz band, as shown in Figure 3.3. The tube open end reflection is within a few dB as shown in Figure 3.6. There are two tube open end transmission estimates as seen in Figure 3.7. The red line is the filter T_L derived above from the external microphone. The green line is amplitude compliment of the estimated R_L filter. Both of these are less accurate below 100 Hz but are extremely accurate from 100 Hz to 10,000 Hz. Comparing the two estimates to each other, the amplitude compliment of R_L performs better above 100 Hz while the external microphone T_L is better when considering the entire band.

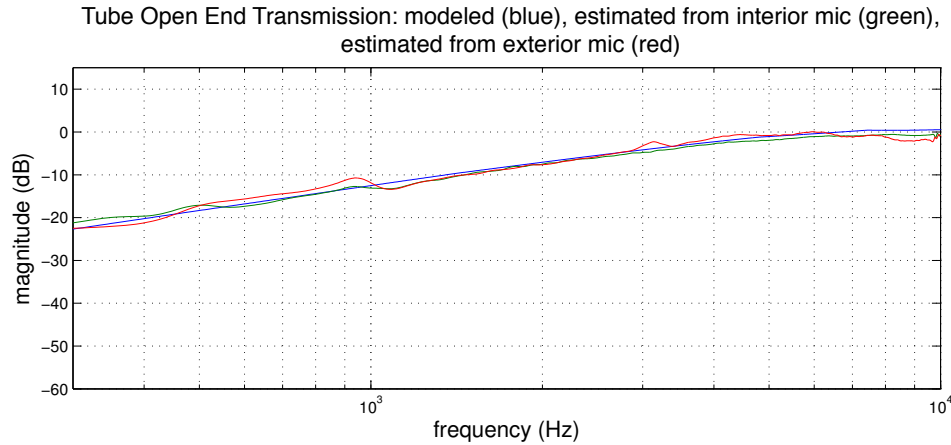


Figure 3.7: Open End Transmission for Tube.

3.5 Appending the Bell

With all of the acoustically significant effects of the tube measured, the tube can be expanded upon and new measurements can be taken. A trombone bell can be attached to the open end of the tube as seen in Figure 3.8. The small end of the bell sets on the larger rim of the PVC tube creating a small junction. Two responses are recorded: B from the co-located microphone and B_E from a microphone suspended 7 cm from the end of the bell flare, shown in Figures 3.9 and 3.10 respectively.

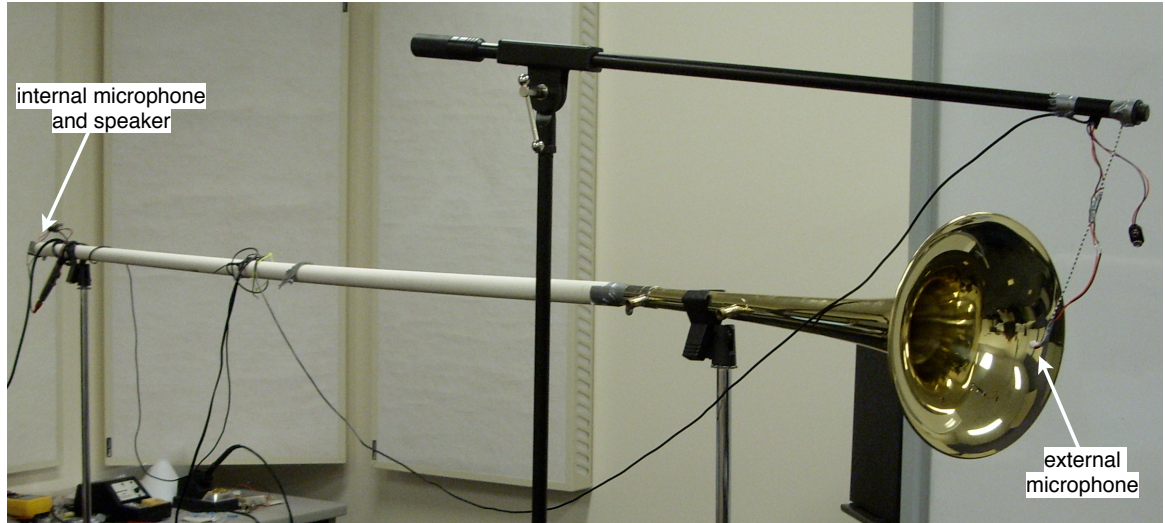


Figure 3.8: The trombone bell appended to the measurement tube.

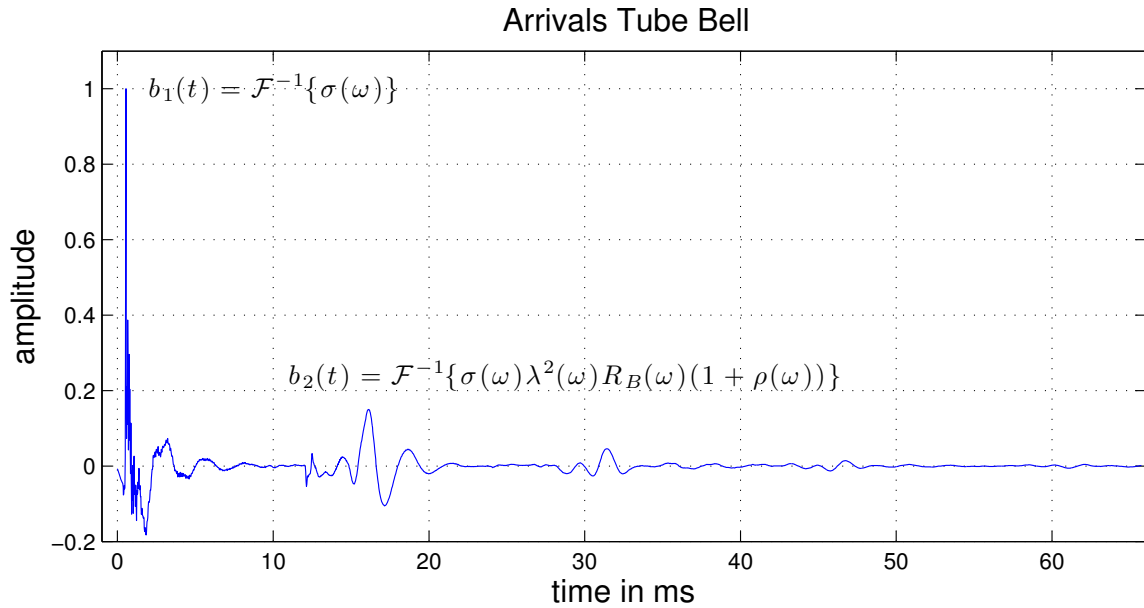


Figure 3.9: Tube with bell appended, internal microphone arrivals.

The process for isolating the trombone bell reflection and transmission are essentially identical to isolating the effects of the open end in the tube. Using the recordings taken from the microphone placed outside of the bell, the transmission filter can also be estimated. The first arrival at the external microphone can be viewed as:

$$B_{E1}(\omega) = \sigma(\omega)\lambda(\omega)T_B(\omega). \quad (3.18)$$

To obtain the T_B :

$$T_B(\omega) = \frac{B_{E1}(\omega)}{\sigma(\omega)\lambda(\omega)}. \quad (3.19)$$

With the measurement system shown to be accurate for estimating known filters, it can now be assumed that the measurements taken for the trombone bell are accurate. The estimated filters for the trombone bell display the general expected behavior, the reflection has a low pass character and the transmission has the opposite high pass character, as shown in Figure 3.11.

In a previous work, [16], the trombone bell was modeled using eight conical sections, with geometry and dimensions determined from the Bessel horn function (2.4) and Table 2.2, using the techniques discussed in the previous chapter.

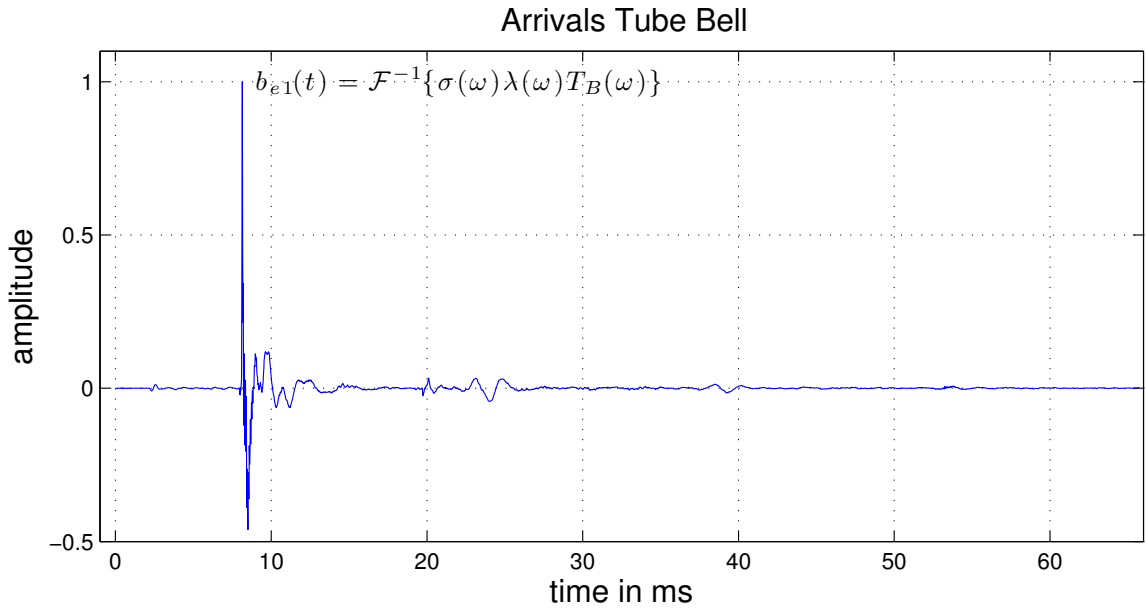


Figure 3.10: Tube with bell appended, external microphone arrivals.

A comparison between the modeled filter and the filter estimated from measurement can be seen in Figure 3.11. It is important to note that unlike the other comparisons in this chapter, the modeled filter is a cruder approximation that does not take into account higher-order and/or evanescent modes present in the bell. With the accuracy of the measurement technique shown earlier in this chapter, it is clear that the differences in the bell reflection spectrum highlight the inadequacies in one-dimensional approximations of bell flares, rather than a failing of the measurement system.

3.6 Frequency Response of the Instrument Model

When the filters discussed in this chapter are added to the waveguide model in Figure 2.2 an impulse of the system can be taken, as all of its components are LTI, the trombone waveguide is also LTI, provided the length of the slide remains static. Each new slide position generates a new impulse response. To evaluate the model's impulse response we must explore the expected acoustical behavior of the trombone. As previously discussed the trombone's bore is primarily a cylindrical tube which is closed off at one end by the player's lip. The fundamental frequency of that tube can be found by $f_0 = c/(4 * L)$ [6],

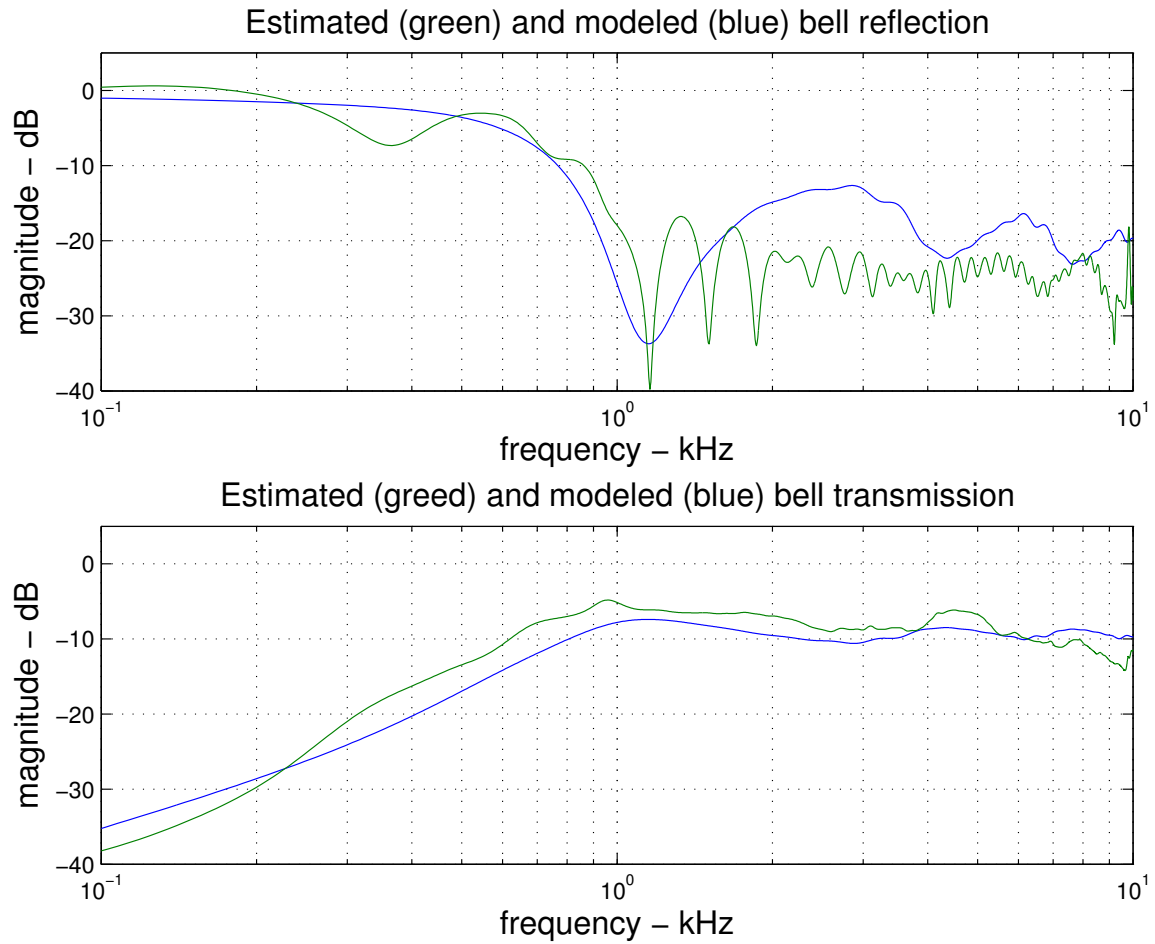


Figure 3.11: Estimated and modeled bell reflection (top) and transmission (bottom) magnitudes.

where c is the speed of sound, (taken as 330 meters per second), and L is the length of tube, approximately 39 Hz for a tube the length of the trombone with the slide retracted, 2.09 meters².

Because of the non-inverting reflection caused by the closed end, the tube will only produce odd harmonics. The frequency response of a model of a 2.09 meter ideal lossless closed cylindrical tube can be seen in top plot in Figure 3.12; note the even 78 Hz gaps between the peaks in relation to the 39 Hz fundamental. The vertical black lines on the

²The length of the bore is calculated by summing the lengths of the parts of the trombone in Table 2.1. When the slide is retracted parts 2 and 4 are equal to 0.

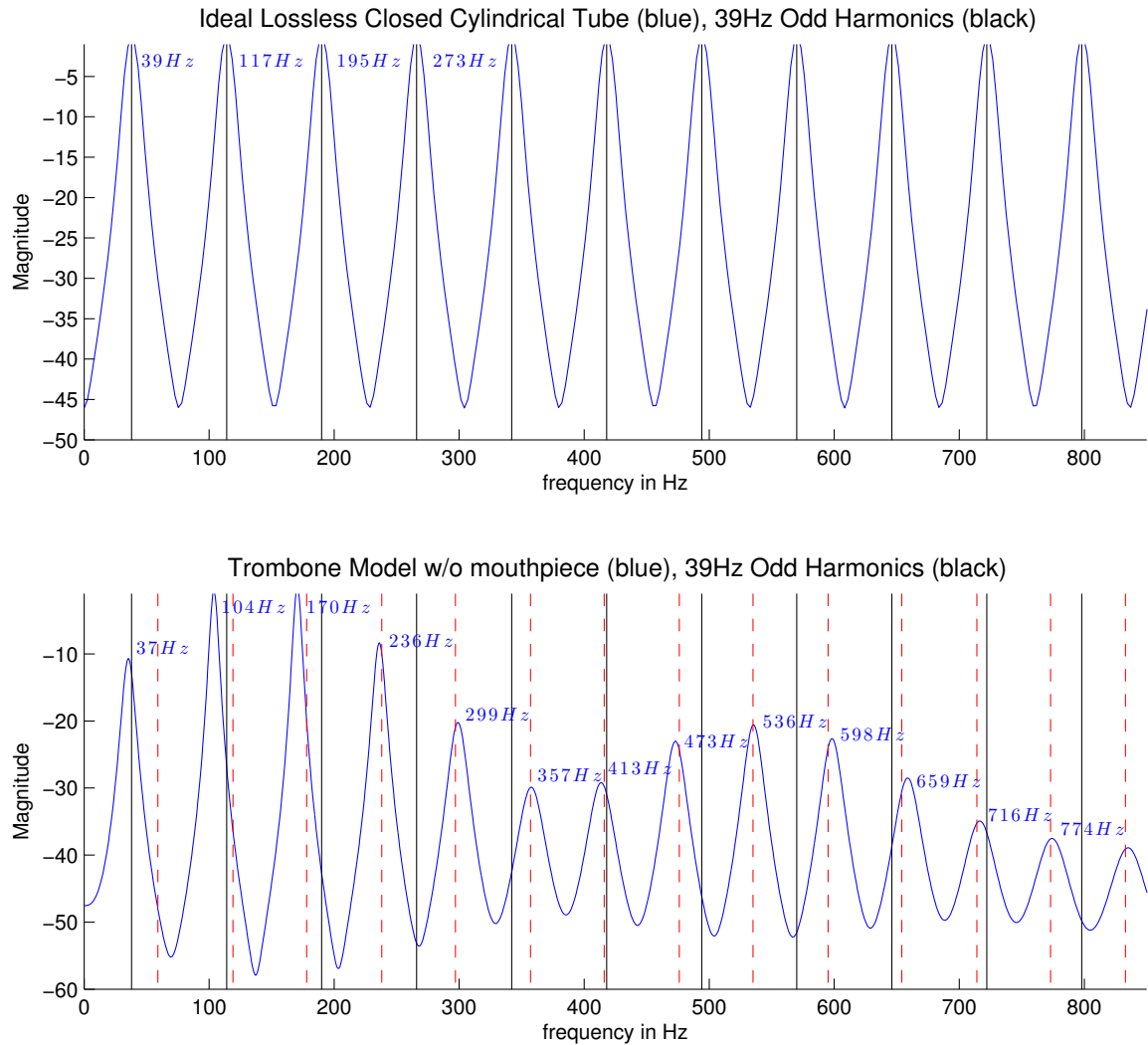


Figure 3.12: Spectrum of the impulse responses of an ideal lossless closed cylindrical tube, the trombone model without a mouthpiece attached with a 39 Hz grid in black and a 60 Hz grid in red.

two graphs in Figure 3.12 are a grid marking the location of the 39 Hz peak at the odd harmonics, e.g. 39, 117, 195 etc. It is shown in the second plot in Figure 3.12 that when the bell is added the higher harmonic peaks are shifted down in frequency to a point where they are no longer integer multiples of the 39 Hz fundamental. These peaks with their dissociation from the fundamental frequency are now more accurately referred to as partials [6]. These bell shifted partials do, however, have a harmonicity as shown with the dotted vertical red lines in Figure 3.12. The third partial and higher are lined up with the 59 Hz grid, forming a new pseudo fundamental frequency for the instrument and form a harmonic series which is complete with the exception of the lowest two components. The standard trombone, pitched in B-flat and with the slide fully retracted, is able to play the notes in the series $59n$ Hz where $n \geq 2$ and an integer. The model here is shown to have strong in-tune partials for $n \geq 3$. The second and first partials are not shifted far enough to be an integer multiple of 59 Hz.

When the trombone's handslide is extended it increases the length of the bore and lowers the fundamental pitch. In Figure 3.13, the length of the bore was increased by 50cm and it appears to have dropped the pseudo fundamental for the higher partials down to approximately 50 Hz from 59 Hz when the slide was fully retracted. Similar to the retracted example, the first two partials were not shifted enough by the bell to fit into the new pseudo fundamental and even the third and fourth partials are not as well in tune as in the retracted example.

After the accurate filters derived in this chapter were inserted into the trombone digital waveguide, the model's impulse response was shown to be behaving in a similar manner to a real trombone. The next step is to make the model produce sound by coupling it with a generalized pressure control valve to simulate the player's lips and additional filters to model the mouthpiece.

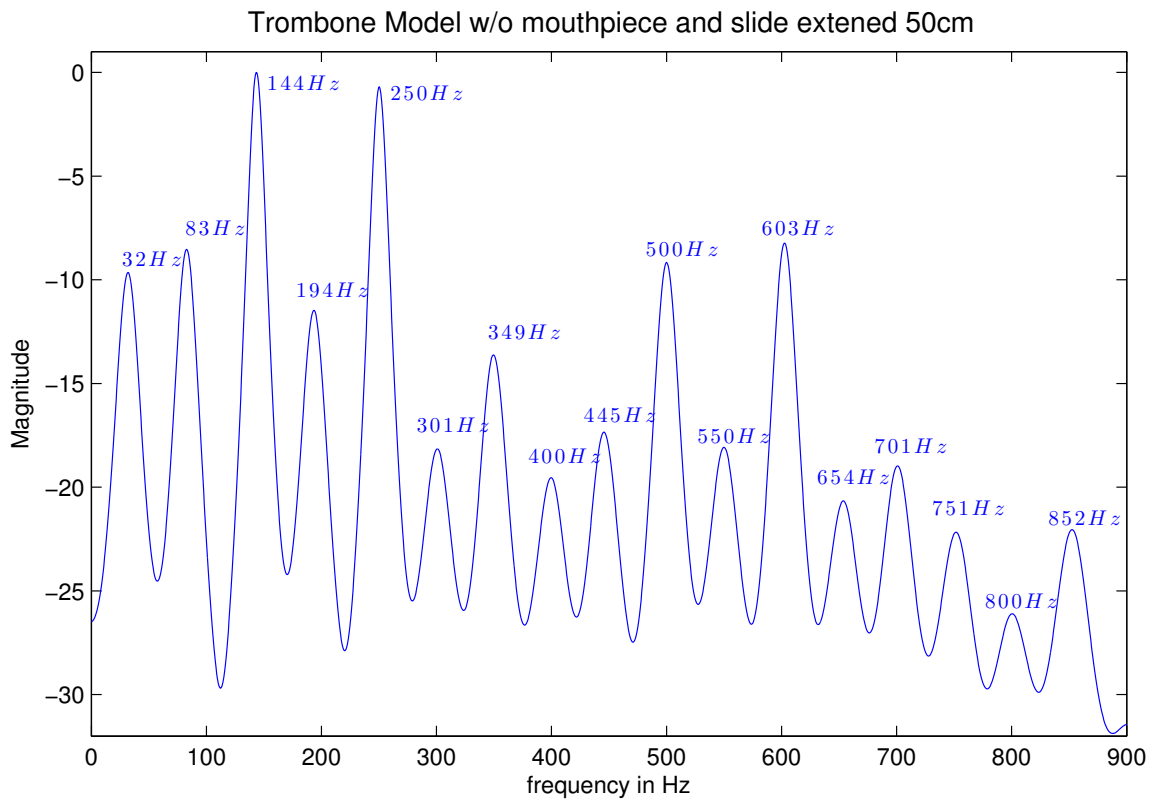


Figure 3.13: Spectrum of the impulse response of the trombone model without mouthpiece and the slide extended 50cm.

Chapter 4

Coupling Lip and Instrument Models

With the waveguide of the bore and bell in place, a mouthpiece and reed model are needed to complete a functional trombone model. The mouthpiece creates a frequency resonance necessary for the trombone's characteristic sound, while the reed model simulates the player's vibrating lips, which provides the input to the instrument.

4.1 The Lip Reed

The trombone is an aerophone, or wind instrument, that is driven by a vibrating reed, a mechanical oscillator that introduces a time varying constriction that modulates the flow of pressure into the instrument bore. There are three types of musically useful reeds, or pressure controlled valves (PCV), that differ in how they open and close in response to pressure, as seen in Figure 4.1. They are described by a couplet, (σ_1, σ_2) , where σ_1 and σ_2 refer to the upstream or downstream behavior of the valve [6]. The values for the couplet can be either + or -, indicating an opening or a closing of the valve, respectively, in the presence of a pressure increase. The three types of valves are: blown closed, $(-, +)$, in which additional upstream pressure tends to close the valve further and additional downstream pressure tends to open the valve further; longitudinally blown open, $(+, -)$, in which additional upstream pressure tends to open the valve further and additional downstream pressure tends to close the valve further; and transversely blown open, $(+, +)$, in which an

increase in either upstream or downstream will tend to open the valve further [6].

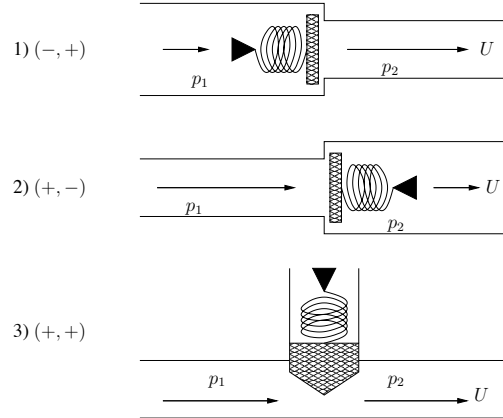


Figure 4.1: Configurations of Pressure Control Valve. 1. blown closed $(-, +)$, found in clarinets and saxophones. 2. longitudinally blown open $(+, -)$, found in trumpets and trombones. 3. transversely blown open $(+, +)$, found in the avian syrinx. [6].

Most single reed woodwind instruments, e.g. clarinets and saxophones, are blown shut PCVs, the pressure from the mouth forces a thin, light cane reed shut until pressure returning from reflections in the bore and bell forces it open again. Brass instruments, e.g. trumpets and trombones, are largely the longitudinally blown open PCVs, as are the human vocal folds. The lips of the player start in a near closed position and are blown open by pressure, originating from the lungs, until pressure returning from the bore closes them again. The transverse blown open PCV is forced open from pressure on from either the mouth or the bore. Some research suggests that the motion of the lips of a brass player playing at higher frequencies is better modeled with the transverse model [1].

In this work, an existing model of a generalized PCV is used [17]. This model abstracts the reed as a single mass set into harmonic motion by the force applied to the surface of the single mass by upstream and downstream pressure. If the reed is modeled as a door swinging on a hinge, as illustrated in Figure 4.2, its motion can be tracked as the angle of displacement, θ , from the fixed point of the vertical axis. For the reed to behave like the lips of a trombone player in the blown open fashion, $(+, -)$, its motion must be restricted by placing a “stop”, an example for which would be fixing the reed’s motion so $\theta \geq 0$, as

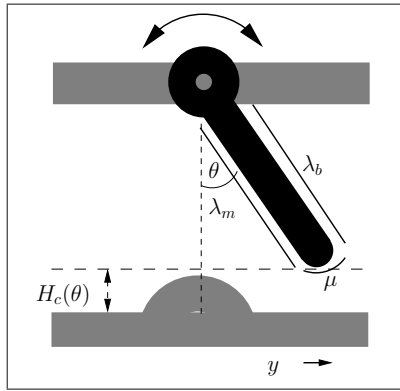


Figure 4.2: Generalized Pressure Control Valve in the blown open configuration with a stop placed on the vertical axis at $\theta = 0$. Parameters λ_m and λ_b are lengths of the reed that are affected by the pressure from the mouth and bore, respectively. μ is the length of the valve that is affected by the volume flow. The forces on these surfaces change the angle of the valve opening, θ .

in Figure 4.2. If a stop is placed at $\theta = 0$, the reed's initial position, θ_0 , is set to the right of the stop, as illustrated in Figure 4.2.

When sufficient pressure is applied from either the mouth or the instrument bore, the reed moves causing the area of the open valve channel, A , to change in accordance with the reed's geometry and configuration:

$$A(\theta) = wH_c(\theta), \quad (4.1)$$

where w is the width of the valve and H_c is the function that gives the height as a function of θ .

$$H_c(\theta; t) = \eta \left| \frac{\theta(t)}{\eta} \right|^\nu, \quad (4.2)$$

in which η is a normalized displacement ratio and ν is the displacement shape exponent. The height function (4.2) is used to simulate more complex motion of the reed than what can be modeled using a single mass. The lips, or embouchure, of a brass player are far from being an ideal Newtonian mass, they deform in three dimensions as they move. In this model the shape of the reed channel is not important for our calculations, only its area, so the width remains fixed while the height function (4.2) attempts to model the lip's complex motion,

while allowing the overall valve model to remain relatively simple and in one dimension [15]. The contours created by different values for ν are illustrated in Figure 4.3. For the produced sound examined in Figures 4.4, a value of 1.4 was used. This results in a smoother opening of the valve that simulated the motion of the lip reed well. For woodwind instruments lower values, such as 0.5, are more suited to modeling the abrupt closure of rigid cane reeds [17].

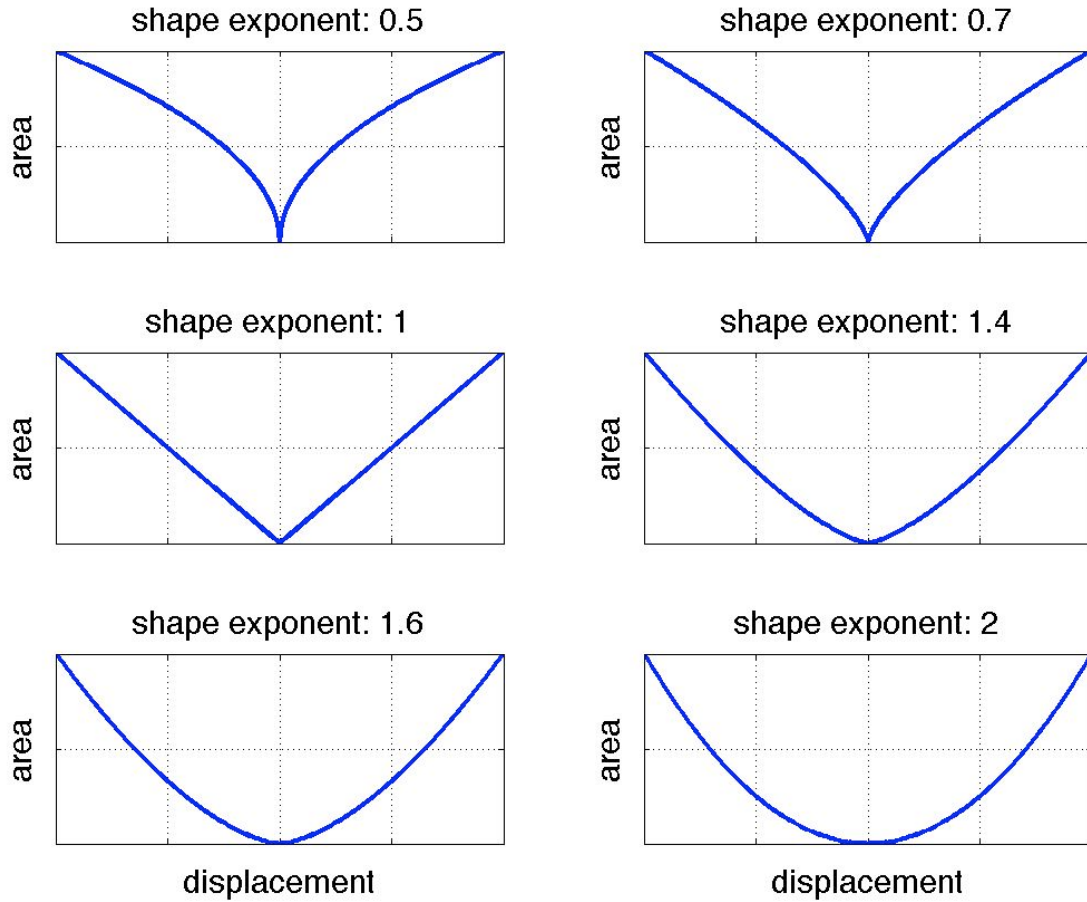


Figure 4.3: Comparison of different ν values used in Equation 4.2.

For the valve area to change the reed must be set in motion. Reed motion is modeled as a single-mass mechanical oscillator with displacement given by the familiar second order differential equation for simple harmonic motion,

$$m \frac{d^2\theta(t)}{dt^2} + m2\gamma \frac{d\theta(t)}{dt} + k(\theta(t) - \theta_0) = F, \quad (4.3)$$

where m is the effective mass of the reed, γ is a damping coefficient, k is the stiffness of the reed and F is the overall driving force acting on the reed, which is governed by the mouth pressure (p_m), bore pressure (p_b) and volume flow ($U(t)$) [17]. Generally, the k value is calculated for a given m after selecting the desired reed resonant frequency, $\omega_v = \sqrt{k/m}$.

When Equation 4.3 is discretized using the Bilinear Transform [13], the reed displacement at discrete time n is determined by

$$\theta(n) = [F_k(n) + 2F_k(n-1) + F_k(n-2) - a_1\theta(n-1) - a_2\theta(n-2)]a_0, \quad (4.4)$$

where

$$\begin{aligned} F_k(n) &= F(n) + k\theta_0, \\ a_0 &= m\alpha^2 + mg\alpha + k, \\ a_1 &= -2(m\alpha^2 - k), \\ a_2 &= m\alpha^2 - mg\alpha + k, \\ \alpha &= 2/T, \\ g &= 2\lambda, \end{aligned}$$

where T is the sampling period [15].

Using the reed displacement, θ , the cross sectional area of the valve channel, $A(t)$, can be found, which can be used to calculate the volume flow, $U(t)$:

$$\frac{dU(t)}{dt} = (p_m - p_b) \frac{A(t)}{\mu\rho} - \frac{U(t)^2}{2\mu(t) + U(t)T}, \quad (4.5)$$

where p_m and p_b are the mouth and bore pressure respectively, and μ is the section of reed affected by the volume flow, U [15].

The reed model can be coupled to the waveguide model by accepting the mouth pressure, p_m and the pressure at the base of the bore $Y_0(t)$, seen in Figure 2.2, as the bore pressure, p_b , creating a pressure differential across the reed that creates volume flow, $U(t)$ and introduces pressure into the instrument. When using proper parameters, such as the examples given in Table 4.1, a stable reed oscillation results, producing the periodic signals seen in Figure 4.4. To produce this the slide was retracted, resulting in an overall bore length of 2.09

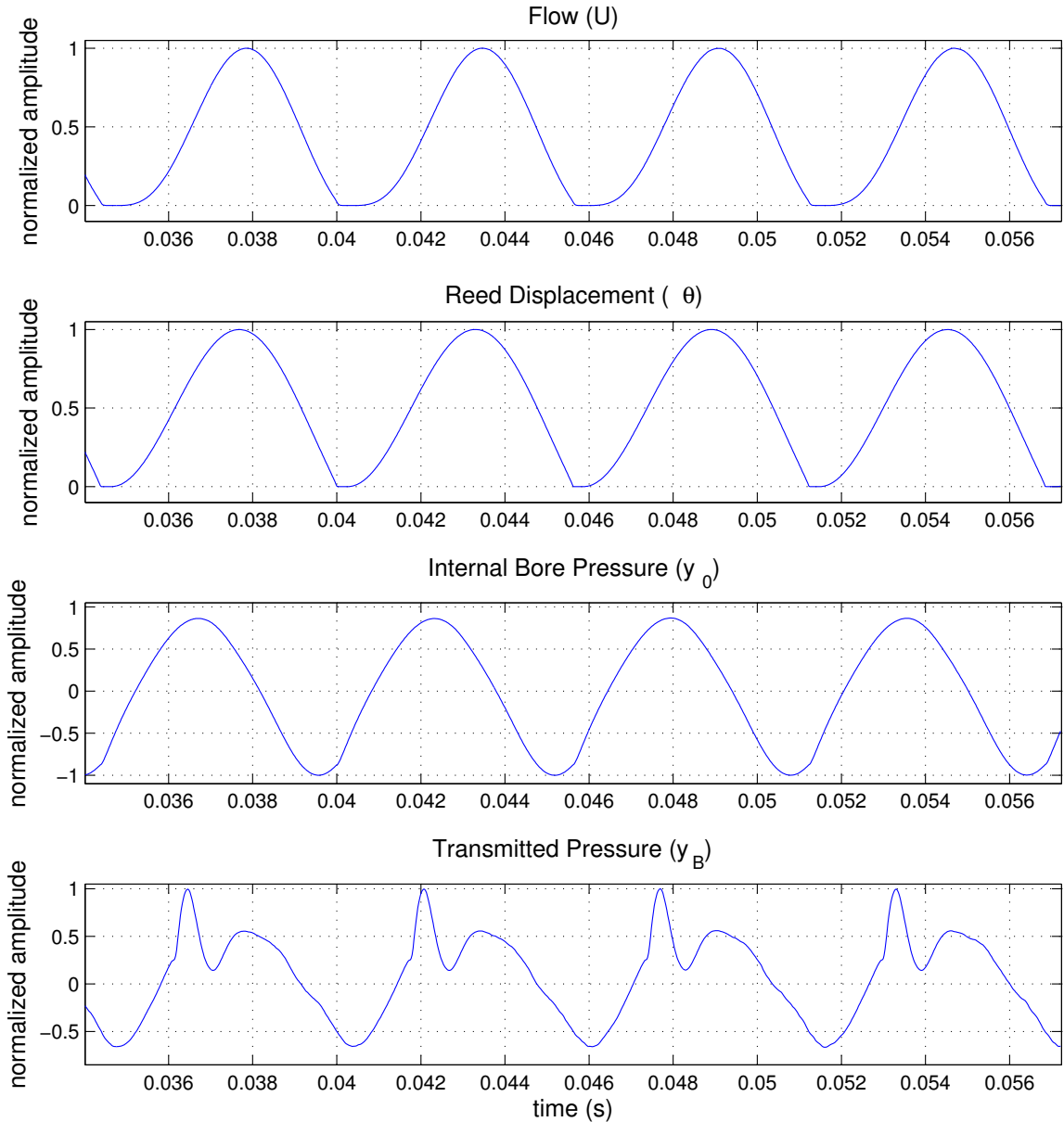


Figure 4.4: Time domain plots of the volume flow, U ; reed displacement, θ ; internal bore pressure, y_0 ; and transmitted pressure, y_b . The outputs for the internal and transmitted pressure correspond to the waveguide model diagram in Figure 2.2.

Quantity	Variable	Value
radius of exhaust	a	8 mm
valve width	w	2.3 mm
valve length	$\lambda_m = \lambda_b$	23.2 mm
valve mass	m	.3 g
valve thickness	μ	6 mm
initial displacement	θ_0	.01 mm

Table 4.1: Example valve parameters [15].

meters, and the reed frequency was set to 156 Hz. When viewed in the time domain, as in Figure 4.4, all four signals (volume flow, U ; reed displacement, θ ; internal bore pressure, y_0 ; transmitted pressure, y_b) have a period of approximately 5 milliseconds, viewing in the frequency domain, seen in Figure 4.5 reveals the fundamental frequency of the produced sound to be 178 Hz. The volume flow, U , reed displacement, θ , and internal bore pressure, y_0 , all have a similar contour, while the transmitted pressure shows the effects of the bell transmission filter's high pass quality. Also the effect of the stop, illustrated in 4.2, on the reed displacement, θ , in Figure 4.5, can be seen restricting it so $\theta >= 0$.

This synthesis example shows that there is not a 1:1 correspondence between the set reed frequency, 156 Hz, the bore frequency, 39 Hz, and the resulting fundamental frequency of the produced sound, 178 Hz. This behavior, problematic when a user desires the instrument to produce a specified pitch, is noted in the literature [1]. Another work sought to solve this problem by creating a mapping of reed frequency to output pitch by finding the unknown reed frequency values for a set of equal temperament pitches using simulated annealing [18].

Further comparison between the produced sound and the instrument model's impulse response, in Figure 4.6, shows that though the resulting sound's harmonic peaks aren't perfectly aligned with the partials of the instrument response, there was enough alignment for the reed to produce a stable oscillation. Also an interesting feature is the relative widths of the peaks of the instrument response versus the produced sound. The sound and its precursor signals, the volume flow $U(t)$ and reed displacement θ have very narrow peaks, as seen in Figures 4.5 and 4.6, while the instrument responses, seen in Figures 3.12 and 4.6, have much wider lobes. It's well known that blown open reeds types can oscillate with some independence from their coupled bore's resonate frequencies, the wider lobes in the

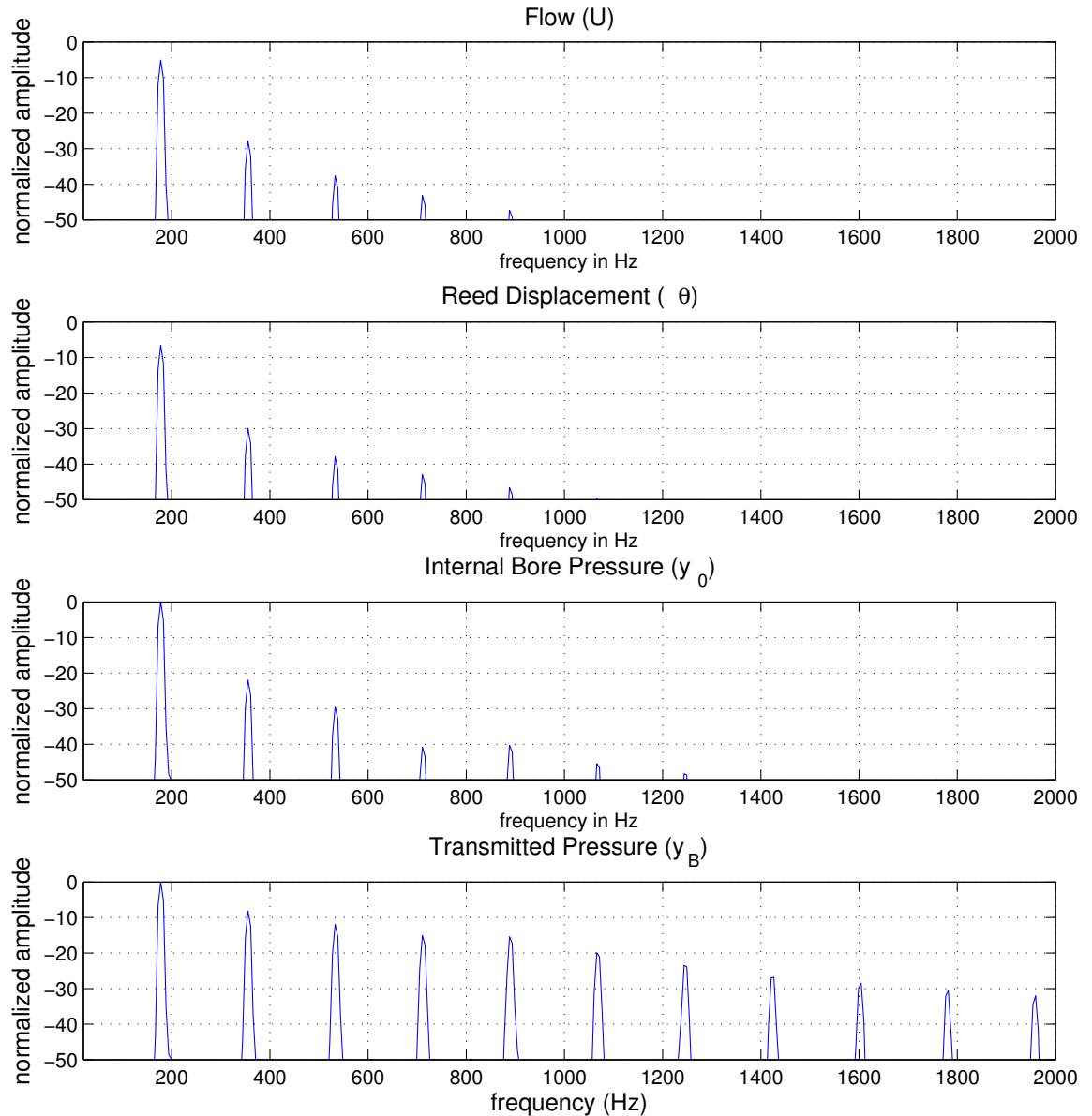


Figure 4.5: Frequency domain plots of the volume flow, U ; reed displacement, θ ; internal bore pressure, y_0 ; and transmitted pressure, y_B . The outputs for the internal and transmitted pressure correspond to the waveguide model diagram in Figure 2.2.

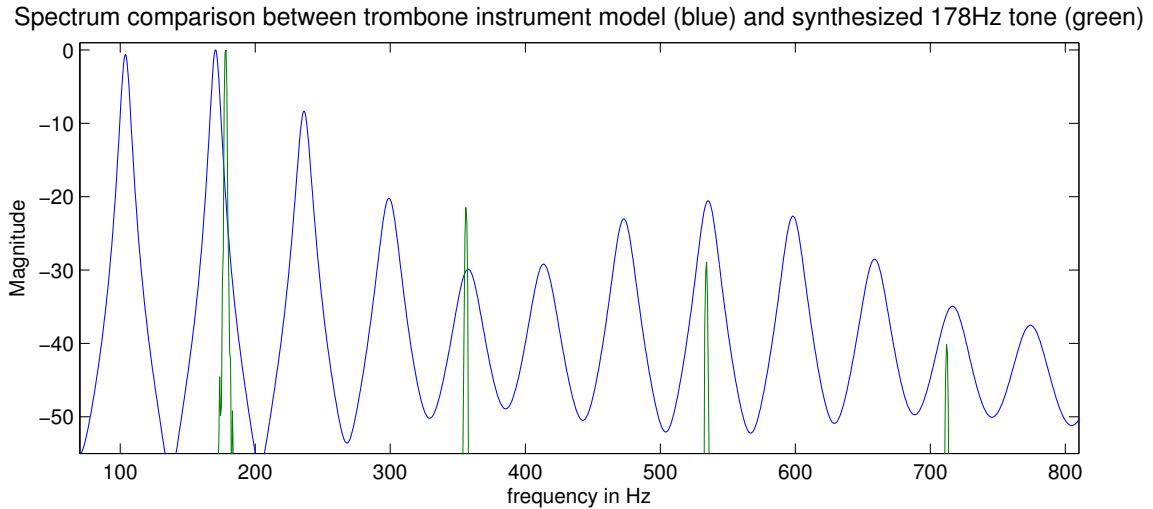


Figure 4.6: Comparison between the frequency spectrum of the trombone instrument model without mouthpiece and the produced sound seen in Figures 4.4 and 4.5.

instrument response could be a partial explanation of this. Experienced brass players are quite familiar with this phenomenon and use it to alter the pitch they are playing using embouchure alone, without changing the length of the instrument bore or shifting to a different partial; this is called bending a note or liping up or down.

4.2 Mouthpiece Formulation

With the bell and main bore accounted for there is only one major acoustical feature that is left unaccounted for, the mouthpiece. This is made up of a cup shaped volume with narrow constriction to a conical backbore as seen in Figure 4.7.

Quantity	Variable	Value
mouthpiece volume	V	$5 \times 10^{-6} m^3$
mouthpiece choke length	l_c	4.8 cm
mouthpiece choke radius	a_c	4.5 mm

Table 4.2: Mouthpiece parameter values [15].

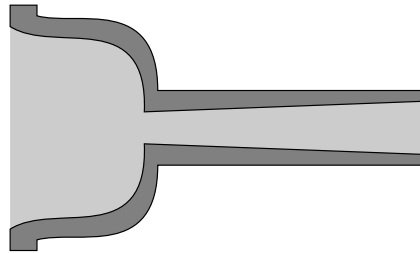


Figure 4.7: Illustration of a mouthpiece cross section, showing the cup shaped volume, V , attached to the conical choke, with length, l_c and an average radius, a_c . Values for these parameters can be found in Table 4.2.

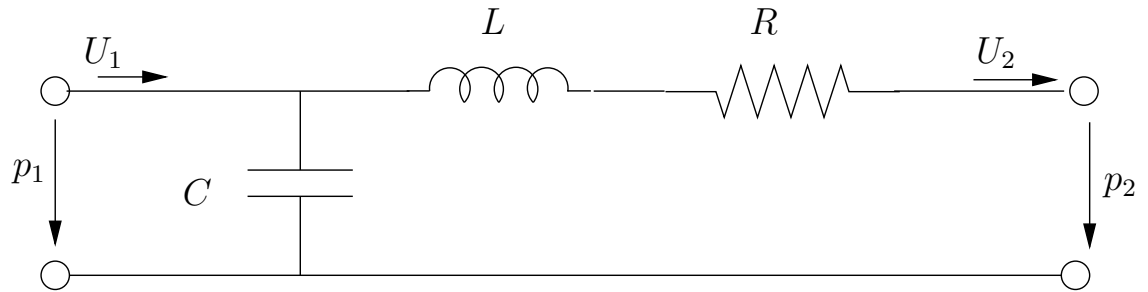


Figure 4.8: The system diagram for the mouthpiece model. The cup volume is represented by the capacitor, and the attached narrow constriction is modeled as a series inertance L and dissipative element R [15].

It is shown in the literature that attempting to model this piecewise with cylinders is not accurate [6]. The current method simulates the effects by mimicking a circuit, as seen in Figure 4.8; the cup with a capacitor, the constriction with series inertance and the cylinder's wall losses with a dissipative element. The mouthpiece cup compliance C is

$$C = \frac{V}{\rho c^2}, \quad (4.6)$$

where V is the volume of the cup, ρ is the air density and c is the speed of sound. The constriction's inertance L is

$$L = \frac{\rho l_c}{S_c}, \quad (4.7)$$

where l_c is its length and S_c is its cross-sectional area. The dissipative value is taken from

the literature [4].

Because the mouthpiece is inserted between the lips and the instrument bore, it changes the upstream volume flow into the bore and the downstream pressure from the bore to the reed, these new mouthpiece affected values are $U_2(t)$ and $p_1(t)$, seen in Figure 4.8. Converse to its outputs, $U_2(t)$ and $p_1(t)$, are the inputs to the mouthpiece the volume flow $U_1(t)$ entering the mouthpiece and the upstream pressure $p_2(t)$ from the reed. Taking the Laplace transform of the differential equations describing the mouthpiece model in Figure 4.8 results in the systems frequency domain input-output matrix

$$\begin{bmatrix} U_1(s) \\ p_1(s) \end{bmatrix} = \begin{bmatrix} s^2 LC + s RC + 1 & sC \\ sL + R & 1 \end{bmatrix} \begin{bmatrix} U_2(s) \\ p_2(s) \end{bmatrix}, \quad (4.8)$$

This matrix formulation can be rearranged and discretized to get equations for $U_2(t)$ and $p_1(t)$, which are given in the z domain as

$$U_2(z) = \frac{U_2(z)(1 + 2z^{-1} + z^{-2}) - C\alpha p_2(z)(1 - z^{-2})}{a_{m0} + a_{m1}z^{-1} + a_{m2}z^{-2}}, \quad (4.9)$$

where

$$\begin{aligned} a_{m0} &= LC\alpha^2 + RC\alpha + 1 \\ a_{m1} &= -2(LC\alpha^2 - 1) \\ a_{m2} &= LC\alpha^2 - RC\alpha + 1, \end{aligned}$$

and

$$p_1(z) = \frac{U_2(z)(b_0 + b_1z^{-1}) + p_2(z)(1 + z^{-1})}{1 + z^{-1}}, \quad (4.10)$$

where

$$\begin{aligned} b_0 &= L\alpha + R \\ b_1 &= -L\alpha + R, \end{aligned}$$

and $\alpha = 2/T$ where T is the sampling period [15].

With the mouthpiece incorporated into the model, its effects can be seen when comparing trombone model impulse response with the mouthpiece to the impulse response of the model without the mouthpiece, seen in Figure 4.9. The mouthpiece reduces the relative distance between the peaks and nulls of the instrument response while also attenuating frequencies above 800 Hz.

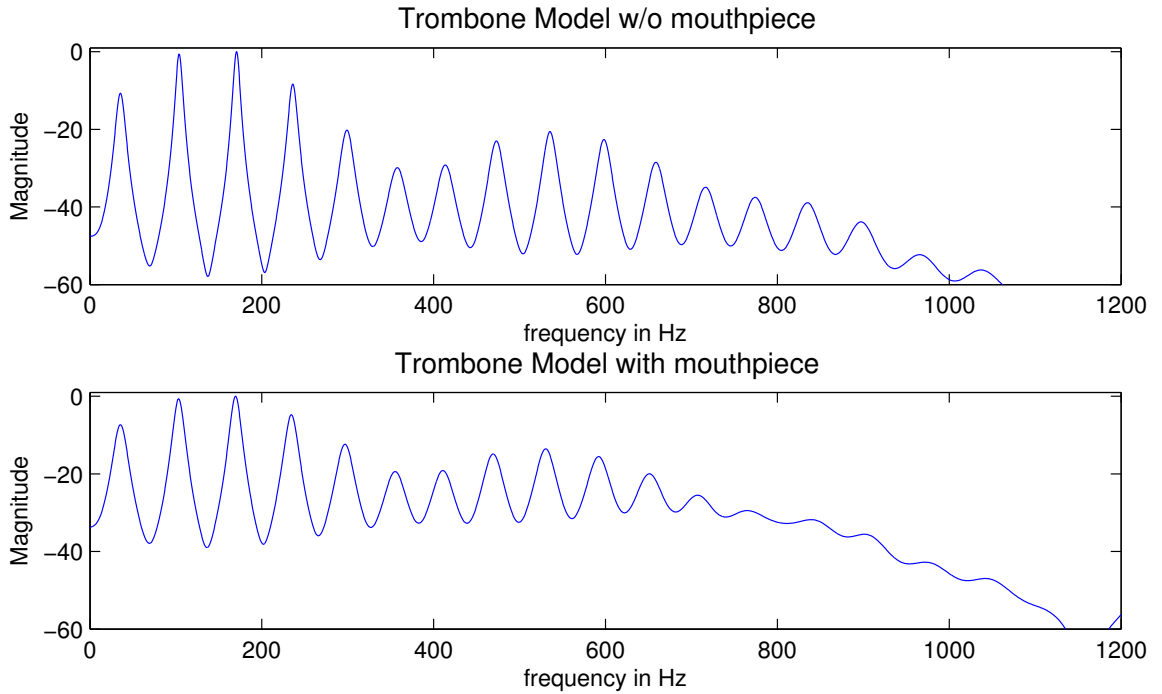


Figure 4.9: Trombone model spectra with and without the mouthpiece.

When comparing the impulse response of the instrument with the mouthpiece with a tone synthesized with that model, in Figure 4.10, it can be seen that much like in Figure 4.6, the narrow resonances of the bore pressure are well supported within the wider frequency lobes of the instrument impulse response.

Spectrum comparison between trombone model w/ mouthpiece (blue) and synthesized 176Hz tone (green)

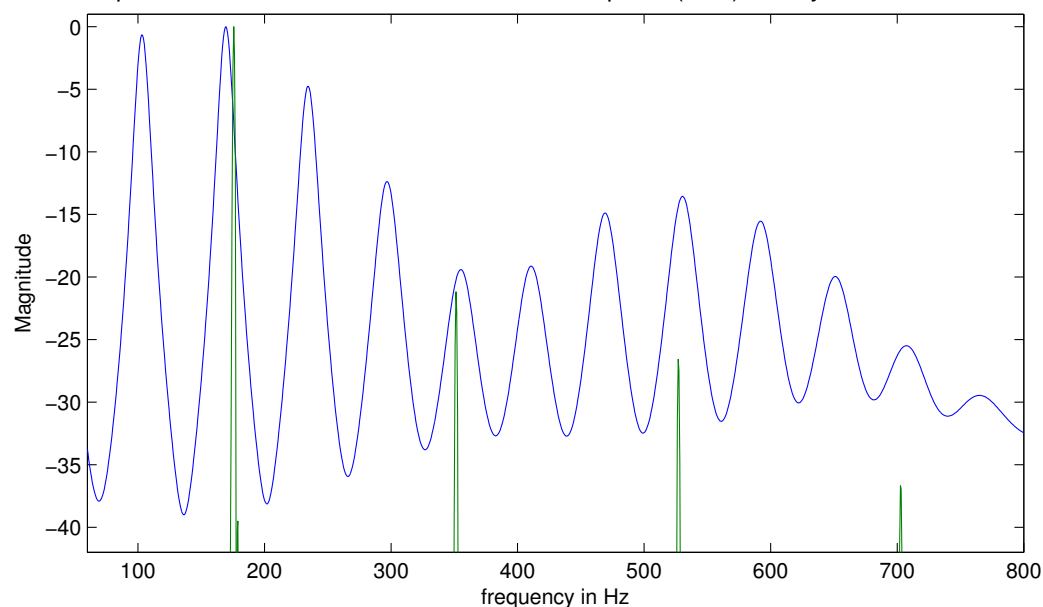


Figure 4.10: Comparison between the frequency spectrum of the trombone instrument model with mouthpiece and a tone synthesized at 176 Hz.

Chapter 5

Conclusion

This work presents a physical synthesis model of the trombone, a parametrically flexible and computationally efficient digital waveguide. Physical modeling is used rather than more traditional signal based synthesis techniques, such as FM or wavetable synthesis, because in addition to creating a model that can produce sounds using intuitive control parameters, the construction and configuration of the model serves as an acoustical study of the instrument and how the player interacts with it.

There are four parts of the trombone to model: the instrument bore, the bell, the lips and the mouthpiece. The cylindrical bore can be seen as an acoustic tube, a structure well known in the literature, that can be efficiently modeled with a bidirectional delay line, a waveguide. The waveguide model of a finite cylindrical tube can be transformed into a simplified trombone model by adding filters accounting for the bell reflection, bell transmission and lip reflection. The effects of the bell flare, which have no known one-dimensional traveling wave solution, unlike the cylindrical tube, may be acoustically measured to overcome the limitations of piecewise approximations.

A previously established measurement technique is used to measure a cylindrical tube in the closed state to remove the acoustic characteristics of the measurement components in the system. The technique is then expanded upon by measuring the cylindrical tube with a trombone bell appended to it. The reasonable assumption of limited linearity and time invariance in the tube and bell systems allow for the taking of their impulse responses. When these impulse responses are viewed in the time domain a pattern of easily separable reflection arrivals can be seen. With the composition of each of these arrivals known, they can be algebraically manipulated to isolate and estimate filters for the waveguide model. The

measured filters for the wall losses, cylindrical open-end reflection and cylindrical open-end transmission very closely match their theoretical expectations. The trombone bell reflection and transmission filters are estimated with this method and are shown to be reasonably similar to their associated piecewise approximations.

To illustrate the effects of the measured bell in context of the whole instrument, the impulse responses of a cylindrical tube, (closed on one end, open on the other), is compared to the trombone model. The cylindrical tube's spectrum has only the odd harmonics of fundamental frequency related to its length. The trombone's spectrum has the same initial fundamental frequency peak as the tube, but all of the higher harmonics are shifted down in frequency, approximating a new harmonic series with a higher fundamental frequency (as described in Section 3.6).

For the trombone waveguide to produce sound a generalized reed model is coupled to the instrument model. This single mass harmonic oscillator uses a configurable height area function to model more complex motion while remaining one dimensional. When sound examples are produced it can be seen that the instrument impulse responses contribute to the periodicity of the reed while filtering its output to a spectrum characteristic of the trombone. Finally, a simulation of the mouthpiece is included that further adds a resonance characteristic of the trombone sound. It is shown that each of the four main elements of the model, bore, bell, lips and mouthpiece, contributes significantly to the instrument.

5.1 Future Work

The measurement technique featured in this work has been used to measure clarinet bells and tenor saxophone bodies. In related work, we also attempted to acoustically measure the entire trombone body, not just the bell. For this a measurement appliance, seen in Figure 5.1, was fashioned that would fit into the trombone inner slide, turning it into a measurement tube similar in purpose to the two meter PVC tube. Unfortunately the inner slide was too short to provide clearly separable arrivals as seen in the figures in Chapter 3, making it difficult to accurately derive filters for elements of the measurement system, something on which the technique relies to accurately estimate waveguide elements.

There are some playability concerns with the model, namely it can be difficult to artfully manipulate the input parameters as an experienced musician would with a real instrument. This concern can be somewhat tempered by considering the real life circumstances of playing

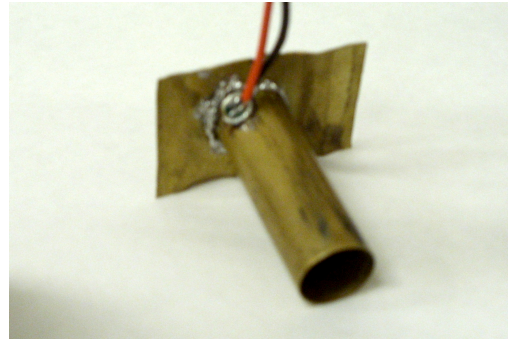


Figure 5.1: Measurement appliance for the trombone inner slide with a microphone capsule flush with the cylinder wall and a backing plate for the mounting of a playback speaker.

the trombone. It can take years for a beginning brass player to develop what is considered to be good tone, let alone be able to play with full expression across the entire range of the instrument. Rather than accepting this and dismissing the model as a viable instrument, it can be seen as an opportunity for future research. Are there feedback mechanisms that could be developed to aid in learning to play the virtual model that carryover in learning to play the real physical instrument? Perhaps there's a new control interface that could be developed to better control of such physical models.

Another avenue of research is exploring the parameter space of the model with inverse modeling or perhaps machine learning. The potential of the instrument is largely untapped because of the difficulty in hand selecting input parameters. If these parameters could be generated by an algorithm or through more complex machine learning techniques, the range of the instrument could be explored. Some progress has been made by others [18], as mentioned previously, but it focussed on optimizing only the output pitch of the instrument by changing the reed frequency. Ideally the full range of input parameters would be open to optimization but this creates problems with high dimensionality. If this could be overcome it would be possible to reconstruct the player's input to the instrument for analysis or to be used as input to another synthesis model, allowing the acoustic instrumentalist to extend their instrument beyond its physical constraints.

Bibliography

- [1] S. Adachi and M. Sato. Trumpet sound simulation using a two-dimensional lip vibration model. *The Journal of the Acoustical Society of America*, 99(2):1200–1209, 1996.
- [2] D. P. Berners. *Acoustics and signal processing techniques for physical modeling of brass instruments*. PhD thesis, Stanford University, 1999.
- [3] P. Cook. Tbone an interactive waveguide brass instrument synthesis workbench for the next machine. In *International Computer Music Conference*, 1991.
- [4] P. Dietz. *Simulation of trumpet tones via physical modeling*. PhD thesis, Dept. of Electrical Engineering, Bucknell University, Lewisburg, USA, 1988.
- [5] A. Farina. Simultaneous measurement of impulse response and distortion with a swept-sine technique. In *Audio Engineering Society Convention 108*, 2 2000.
- [6] N. H. Flechter and T. D. Rossing. *The Physics of Musical Instruments*. Springer-Verlag, 1995.
- [7] D. A. Jaffe and J. O. Smith. Extensions of the karplus-strong plucked-string algorithm. *Computer Music Journal*, 7(2):pp. 56–69, 1983.
- [8] K. Karplus and A. Strong. Digital synthesis of plucked-string and drum timbres. *Computer Music J.*, 7(2):43–55, 1983.
- [9] X. Rodet and C. Vergez. Physical models of trumpet-like instruments, detailed behavior and model improvements. In *Proceedings of the International Computer Music Conference*, pages pp. 448–453, 1996.
- [10] J. O. Smith. *Music Applications of Digital Waveguides*. Tech. Rep. STAN-M-39, CCRMA, Stanford University, CA, 1987.
- [11] J. O. Smith. *Introduction to Digital Filters: With Audio Applications*. W3K Publishing, 2007.
- [12] J. O. Smith. *Mathematics of the Discrete Fourier Transform (DFT)*. W3K Publishing, 2007.

- [13] J. O. Smith. *Physical Audio Signal Processing*. W3K Publishing, 2010.
- [14] T. Smyth. Estimating waveguide model elements from acoustic tube measurements. *Acta Acustica united with Acustica*, 95:1093–1103(11), November/December 2009.
- [15] T. Smyth and F. S. Scott. Parametric trombone synthesis by coupling dynamic lip valve and instrument models. In *Sound and Music Computing Conference*, 2011.
- [16] T. Smyth and F. S. Scott. Trombone synthesis by model and measurement. *EURASIP Journal on Advances in Signal Processing*, 2011(1):151436, 2011.
- [17] J. S. Abel T. Smyth and J. O. Smith. A generalized parametric reed model for virtual musical instruments. In *International Computer Music Conference*, pages pp. 347–350, 2005.
- [18] C. Vergez and P. Tisserand. The brass project, from physical models to virtual musical instruments: Playability issues. In *Computer Music Modeling and Retrieval*, volume 3902, pages 24–33. Springer Berlin / Heidelberg, 2006.